GEOLOGICA CARPATHICA, FEBRUARY 2016, 67, 1, 3–20 doi: 10.1515/geoca-2016-0001

Fluid evolution and mineralogy of Mn-Fe-barite-fluorite mineralizations at the contact of the Thuringian Basin, Thüringer Wald and Thüringer Schiefergebirge in Germany

JURAJ MAJZLAN[1]✉, MARIA BREY-FUNKE[1], ALEXANDER MALZ[1], STEFAN DONNDORF[1] and RASTISLAV MILOVSKÝ[2]

[1]Institute of Geosciences, Friedrich Schiller University, Carl-Zeiss Promenade 10, D-07745 Jena, Germany; ✉Juraj.Majzlan@uni-jena.de
[2]Earth Science Institute of the Slovak Academy of Sciences, Ďumbierska 1, SK-974 01 Banská Bystrica, Slovakia

(Manuscript received July 4, 2015; accepted in revised form October 1, 2015)

Abstract: Numerous small deposits and occurrences of Mn-Fe-fluorite-barite mineralization have developed at the contact of the Thuringian Basin, Thüringer Wald and Thüringer Schiefergebirge in central Germany. The studied mineralizations comprise the assemblages siderite+ankerite-calcite-fluorite-barite and hematite-Mn oxides-calcite-barite, with the precipitation sequence in that order within each assemblage. A structural geological analysis places the origin of the barite veins between the Middle Jurassic and Early Cretaceous. Primary fluid inclusions contain water vapour and an aqueous phase with NaCl and $CaCl_2$ as the main solutes, with salinities mostly between 24–27 mass. % $CaCl_2$ eq. T_h measurements range between 85 °C and 160 °C in barite, between 139 °C and 163 °C in siderite, and between 80 °C and 130 °C in fluorite and calcite. Stable isotopes (S, O) point to the evaporitic source of sulphur in the observed mineralizations. The S,C,O isotopic compositions suggest that barite and calcite could not have precipitated from the same fluid. The isotopic composition of the fluid that precipitated barite is close to the sea water in the entire Permo–Mesozoic time span whereas calcite is isotopically distinctly heavier, as if the fluids were affected by evaporation. The fluid evolution in the siliciclastic/volcanic *Rotliegend* sediments (as determined by a number of earlier petrological and geochemical studies) can be correlated with the deposition sequence of the ore minerals. In particular, the bleaching of the sediments by reduced *Rotliegend* fluids (basinal brines) could be the event that mobilized Fe and Mn. These elements were deposited as siderite+ankerite within the *Zechstein* carbonate rocks and as hematite+Mn oxides within the oxidizing environment of the Permian volcanic and volcanoclastic rocks. A Middle-Jurassic illitization event delivered Ca, Na, Ba, and Pb from the feldspars into the basinal brines. Of these elements, Ba was deposited as massive barite veins.

Key words: hydrothermal mineralization, fluid inclusion, stable isotopes, Thuringian basin.

Introduction

The Thuringian Basin is an 80×160 km wide syncline, slightly elongated along a NW–SE axis, formed by Permian to Triassic strata with a total thickness of up to 2.5 km. The basin is situated in the central part of the state of Thuringia (central Germany) and is bordered by the Harz Mountains to the north and the Thüringer Schiefergebirge and Thüringer Wald to the south (Thomson & Zeh 2000; Fig. 1). These large basement-cored anticlines and uplifted blocks were deformed during the Late Cretaceous compressional event, which affected large areas of western and central

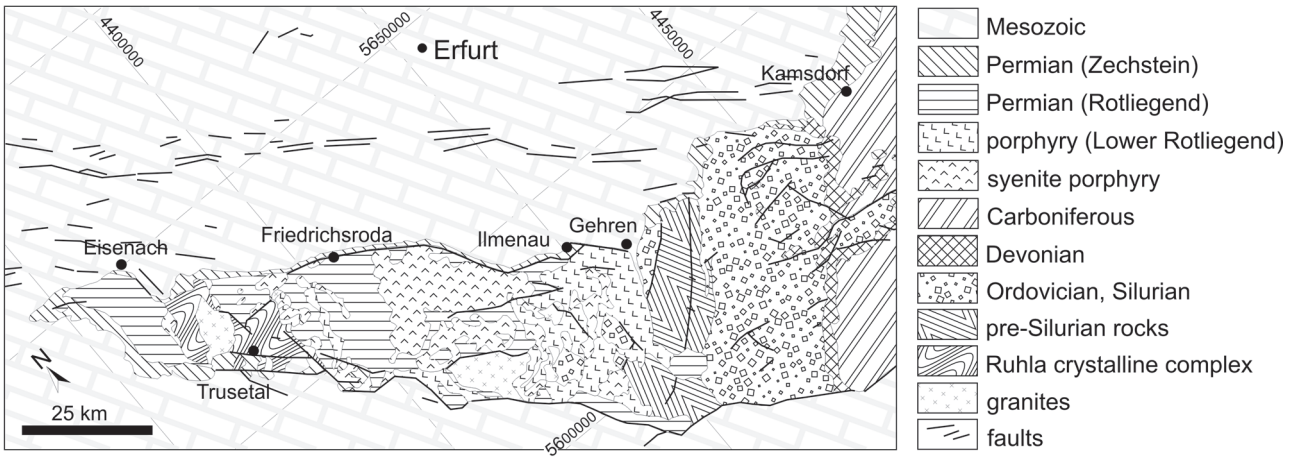

Fig. 1. A simplified geological map of Thüringen, displaying the location of the sampled deposits.

Europe (Schröder 1987; Ziegler 1987; Kley & Voigt 2008). The contractional deformation is often suspected to initiate the migration of fluids from the basement upward (Meinel 1993) and the large-scale fluid circulation is thought to have led to the formation of numerous hydrothermal deposits along the margins of the Thuringian Basin (Rüger & Decker 1992). These deposits were economically exploitable, particularly in the southern area of the basin, and have been mined since the Middle Ages (Zimmermann 1914).

Some of the more important ore deposits are situated in the Saalfeld-Kamsdorf region where a total of 1.4 million tons of iron ore were mined from 1715 to 1867 (Beyschlag 1988); the Ilmenau region where 2.9 million tons of fluorite and barite were excavated from the Floßberg vein alone between 1950 and 1991; and the Hühn region (Trusetal) where iron ore, fluorite, and barite were excavated from the 16th century to 1968. Persistent economic interest in these deposits stimulated a number of scientific studies over the last 40 years in order to understand their mineralogy, structural geology, reserves, and, to a lesser extent, their origin and fluid chemistry.

Equally historically important were the oxidic and silicate manganese ores, mined in the wider vicinity of the township of Ilmenau. The first written documents about the ore exploitation here date back to 1668 and 1732 and the mining ceased in 1949. About 44,700 tonnes of the Mn ores were extracted in the Arlesberg district and the remaining reserves are considered to be negligible.

The mineralizations on the southern edge of the Thuringian Basin bear a number of similar features to numerous deposits and occurrences throughout post-Variscan Europe, such as deposits in France (Charef & Sheppard 1988; Munoz et al. 1994, 2005; McGaig et al. 2000), Spain (Halliday and Mitchell 1984; Wickham & Taylor 1990; Canals and Cardellach 1993; Galindo et al. 1994; Subías and Fernández-Nieto 1995; Johnson et al. 1996; Crespo et al. 2002; Piqué et al. 2008), Sardinia (Muchez et al. 2005; Boni et al. 2009), Germany (Behr & Gerler 1987; Mertz et al. 1989; Boness et al. 1990; Lüders & Möller 1992; Meinel 1993; Hähnel et al. 1995; Krahn & Baumann 1996; Meyer et al. 2000; Zeh & Thomson 2000; Wagner & Lorenz 2002; Schwinn et al. 2006; Baatartsogt et al. 2007; Staude et al. 2007, 2011; Wagner et al. 2010), Poland (Leach et al. 1996; Heijlen et al. 2003; Schmidt-Mumm & Wolfgramm 2004), Slovakia (Hurai et al. 2002, 2008), Belgium (Slobodnik et al. 1994), Hungary (Benkó et al. 2014), Czech Republic (Kučera et al. 2010), England (Gleeson et al. 2000) and Ireland (O'Reily et al. 1997). All these deposits show similarity in some common parameters, such as their age, fluid chemistry, stable isotopes, mineralization styles and their mineralogical and geological background.

Modern, active systems and analogues of these deposits can be also found, for example in the geothermal field of Soultz-Sous-Forêts (France) and the Rhein graben (Scheiber et al. 2012). A large-scale circulation of the hydrothermal fluids significantly affects the geothermal gradient in the area (Genter et al. 2010, their fig. 8) and causes alteration of the host rocks. The fluids at this site are currently precipitating barite-celestite solid solution, galena, and other sulphides (Nitschke et al. 2014).

Here we present an analysis of fluid inclusions of the studied mineralizations. The fluid inclusion data are given together with further mineralogical and geochemical data from the ores in order to develop a sequence of events compatible with the regional tectonic evolution of the Thuringian Basin. We link the mineralizations to the evolution of the Permian siliciclastic rocks. This link may account for the observations made in this and other studies and explains well the timing, geochemistry, and mineralogy of the studied ore deposits.

In this study, we have analysed several hydrothermal deposits located in a belt along the southern edge of the Thuringian basin. Most of these deposits were mined between the 16th and mid-20th century and are no longer accessible today. Hence, much historical information has been drawn from the literature, written by those who saw these veins in the spectacular underground outcrops.

According to Hähnel et al. (1995) and Baumann & Leeder (1969), the earliest mineralization of the studied hydrothermal vein deposits are sparse veinlets of quartz, hematite, and locally small amounts of carbonates coloured red by finely dispersed hematite. According to the observations in the *Sächsisches Erzgebirge*, Schröder (1970) assigned late Variscan–Permian age to this quartz-hematite-ankerite mineralization.

The precipitation of quartz, hematite, and the carbonates was followed by the deposition of ankerite. According to Kling (1995), ankerite replaced the *Zechstein* limestones and is limited to the largest faults and their vicinity. Afterwards, the *siderite+ankerite* assemblage studied here formed. It is represented by large metasomatic bodies of siderite and ankerite in the *Zechstein* carbonates or in the earlier ankerite. Siderite occurs also as veins and is spatially bound to the *Zechstein* strata and found in the marginal areas of both the *Thüringer Schiefergebirge* and *Thüringer Wald*. Deposits developed in the Paleozoic basement, for example *Gehren,* do not contain siderite. In these deposits, calcite is the major carbonate mineral. Meinel (1993) and Franzke and Schiemenz (1980) attribute the absence of siderite and ankerite to the highly oxidizing environment within the abundant Permian volcanics and sediments in this area.

The siderite mineralization is thought to be connected with the mid-Mesozoic extension stage whose main activity is traceable in the Upper Jurassic–Lower Cretaceous (Hähnel et al. 1995; Thomson & Zeh 2000). After the emplacement of the siderite mineralization, the tectonic regime changed in the late Cretaceous–Tertiary to contractional strain. White calcite replaced siderite and formed as lenses up to 15 m thick. In the Gehren region, calcite is later accompanied by fluorite. The main phases of fluorite and barite deposition postdate calcite precipitation. In the wide geographic region of the Thuringian Basin and the adjacent geological units, barite and fluorite are thought to be related to the upper Cretaceous uplift, either in the *Harz* Mountains (Lüders & Möller 1992), the Thüringer Wald (Zeh & Thomson 2000), or in the Thüringer Schiefergebirge (Meinel 1993).

The deposition of fluorite, however, is limited to the marginal areas between the Thuringian Basin and the Harz

Mountains (Lüders & Möller 1992) and the Thuringian Basin and the Thüringer Wald. Fluorite is missing at the interface of the basin and the Thüringer Schiefergebirge, except for the circumference of the two intrusive granitoid complexes (Sparnberger Granit, Henneberggranit). An explanation for the absence of fluorite is the low total F content of the rocks of the Thüringer Schiefergebirge (Meinel 1993).

The barite-fluorite veins, steep vertical or shallow horizontal lenses reach a thickness of up to 10m. Distinct replacement patterns can be observed throughout the deposits — fluorite replaces calcite (Hähnel et al. 1995; Kießling 2007) and barite replaces fluorite. In addition, there are hints of multiple deposition of barite in specific tectonic pulses — "seismic pumping" (Meinel 1993; Hähnel et al. 1995).

The latest mineralogical overprint is represented by the anhydrite-quartz veins with a thickness of up to 10 m, especially in the Hühn area. Anhydrite replaces calcite and siderite. There is no anhydrite mineralization except for a few relics in the Kamsdorf region. The youngest hydrothermal event is pervasive silicification. Quartz replaces preferably anhydrite (if existing) but also siderite and ankerite.

Materials and methods

Samples of hydrothermal sulphides, Mn oxides and silicates, calcite, fluorite, ankerite, siderite, and barite from the southern edge of the Thuringian basin were investigated (Fig. 1). Most of the samples were collected in the field and complemented with selected samples from the Mineralogical Collection of the University of *Jena* and of the *Thüringer Landesamt für Umwelt und Geologie*, Weimar. The collected samples were prepared for petrographic observations as standard thin and polished sections. They were studied in transmitted and reflected polarized light prior to further analyses.

Microthermometry

Fluid inclusions were observed and analysed in 23 doubly polished sections (200–300 μm thick) of barite, calcite (from *Gehren* region), fluorite, and siderite (from *Hühn* region). Phase transitions (melting temperature of ice, $T_{m,ice}$; melting temperature of hydrohalite, $T_{m,hydrohalite}$; eutectic temperature, T_e; temperature of total homogenization, T_h) in fluid inclusions were measured using a Linkam THM 600 programmable freezing-heating stage mounted on a ZEISS AXIOPLAN microscope. A digital JVC camera, long-working-distance Nikon objectives with magnifications of 20×, 32× and 50×, and an image analysing system were used to visualize the inclusions on a computer screen. The stage was calibrated against the phase transitions of three pure chemical compounds with known transition temperatures: the triple point of CO_2 (–56.6 °C) in natural fluid inclusions (previously checked by Raman spectroscopy to contain only CO_2 in the gas phase), the melting temperature of H_2O (0.0 °C), and the melting temperature of sulphur (119.2 °C). The reproducibility of measurements was within ±0.1 °C for the cryogenic temperatures and ±1–2 °C for the T_h measurements. Temperatures of phase transitions were always measured upon heating using a heating rate of 0.1° C/min.

The salinities were calculated from the measured final ice melting temperature of aqueous two-phase inclusions with the Aqso2e program of Bakker (2009) based on the equations of Naden (1996). The salinity of the fluids is given here in $CaCl_2$ eq. wt% to express all data in one single salt system. For the NaCl-$CaCl_2$-H_2O-system, salinities were calculated as NaCl (eq. mass%) and $CaCl_2$ (eq. mass%) equivalents, for which the final melting temperatures of ice ($T_{m,ice}$) and hydrohalite ($T_{m,hydrohalite}$) were needed (after Steele-MacInnis et al. 2011).

Stable isotope analysis

The stable isotope compositions of barite and anhydrite samples were analysed at the isotope laboratory of the *TU Bergakademie Freiberg*. Mineral separates of the sulphates were hand-picked under a binocular microscope, followed by cleaning in doubly distilled water to remove any water-soluble impurities. The sulphates were measured using procedures given in Giesemann et al. (1994). The sulphur isotope compositions of the mineral separates were analysed using an elemental analyser (Fisions CarloErba) coupled to the mass spectrometer (CF-IRMS-Delta plus ThermoQuest-Finnigan). The $\delta^{18}O$ values of $BaSO_4$ and $CaSO_4$ were analysed using a high-temperature pyrolysis system from HEKAtech (Kornexl et al. 1999) coupled to continuous flow isotope ratio mass spectrometry (CF-IRMS-Delta plus ThermoQuinn-Finnigan). Isotope ratios are reported as $\delta^{18}O$ and $\delta^{34}S$ values in per mil (‰) relative to the V-SMOW and V-CDT standards, respectively. Standards used for the system calibration were IAEA-SO-5 and IAEA-SO-6 for oxygen isotopes and IAEA-S-2, IAEA-S-3 and NBS 127 for sulphur isotopes (Kornexl et al. 1999; Ding et al. 2001). Every sample was measured at least three times. The reproducibility of oxygen isotopes from sulphate is better than 0.5 ‰ and the reproducibility of the $\delta^{34}S$ measurements was better than 0.3 ‰, although the internal error of three successive measurements was often smaller.

Carbon and oxygen isotopes of carbonates were measured with an automated carbonate preparation system Gasbench coupled to isotope ratio mass spectrometer MAT253 (Thermo). Powdered samples of ca. 600–800 mg were flushed with helium in septum-sealed glass vials, then reacted with anhydrous H_3PO_4 for 24 hours at 25 °C. The CO_2 yield was chromatographically separated and introduced into a mass spectrometer in continuous flow mode (helium as carrier gas), whereby three injections of reference gas are followed by four injections of sample aliquots. A set of working standards, traceable to international standards were regularly scattered between samples to check for accuracy. The usual precision of the method is 0.2 ‰ for $\delta^{18}O$ and 0.1 ‰ for $\delta^{13}C$.

Powder X-ray diffraction (pXRD)

All samples from the Mn oxide-silicate mineralization and selected samples from the barite-fluorite mineralization were

ground to powder and front-loaded in plastic sample holders. pXRD data were collected with a Bruker (D8 AXS Advance DaVinci) diffractometer, equipped with a Cu X-ray source and operating at 40 kV and 40 mA. The pXRD patterns were compared to the database entries in the PDF 2.0 database, using the Bruker software EVA.

X-ray fluorescence (XRF) analysis

The bulk chemical composition of selected samples (especially the samples from the Mn-Fe mineralization) was measured with an XRF spectrometer Philips (PW 2404) in the wavelength-dispersive mode. The samples were ground to analytical fineness, thoroughly mixed with wax (sample:wax ratio of 4:1), pressed into pellets in a hydraulic press under the load of 294.2 kN, and dried for 24 hours at 45 °C.

Results

Structural geological settings

Saalfeld-Kamsdorf

The Kamsdorf ore field is situated at the contact of the Thuringian Basin to the Thüringer Schiefergebirge (Figs. 1, 2) and hosts barite and sulphide ore mineralizations within repeatedly deformed rocks. The rocks are of Upper Permian (*Zechstein*) age and are mildly tilted (~3°) to the north. In the Kamsdorf ore field, we recognized two main events of brittle deformation (Fig. 3), each with a different direction and kinematics, and one main event of mineralization (Fig. 4). The first event is associated with the formation of normal faults and conjugated shear fractures, suggesting vertical orientation of the maximal stress (σ_1). Hence, the settings, which formed these structures, can be interpreted in terms of an extensional regime. According to the mean trending direction of the normal faults striking NW–SE (Fig. 4), the tensional stress (σ_3) was very likely oriented NE–SW, coinciding with the results of earlier studies on the stress evolution in Thuringia (Rauche & Franzke, 1990).

The second deformation event is characterized by the formation of thrust faults and the reverse reactivation of normal faults. In the Kamsdorf region, the contractional structures

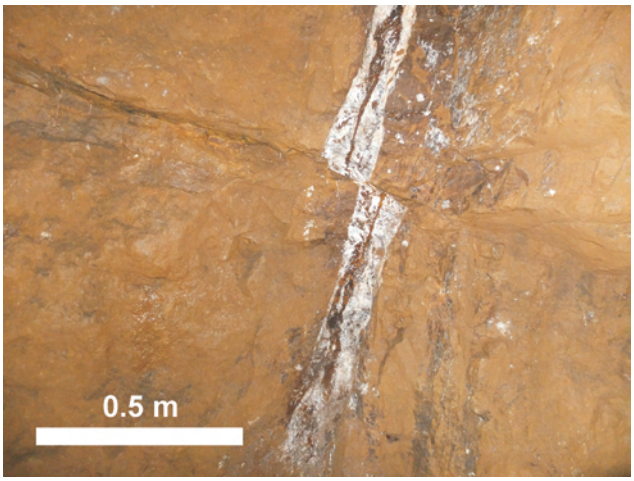

Fig. 3. Barite vein from Kamsdorf, offset by the compressional tectonic events related to the basin inversion.

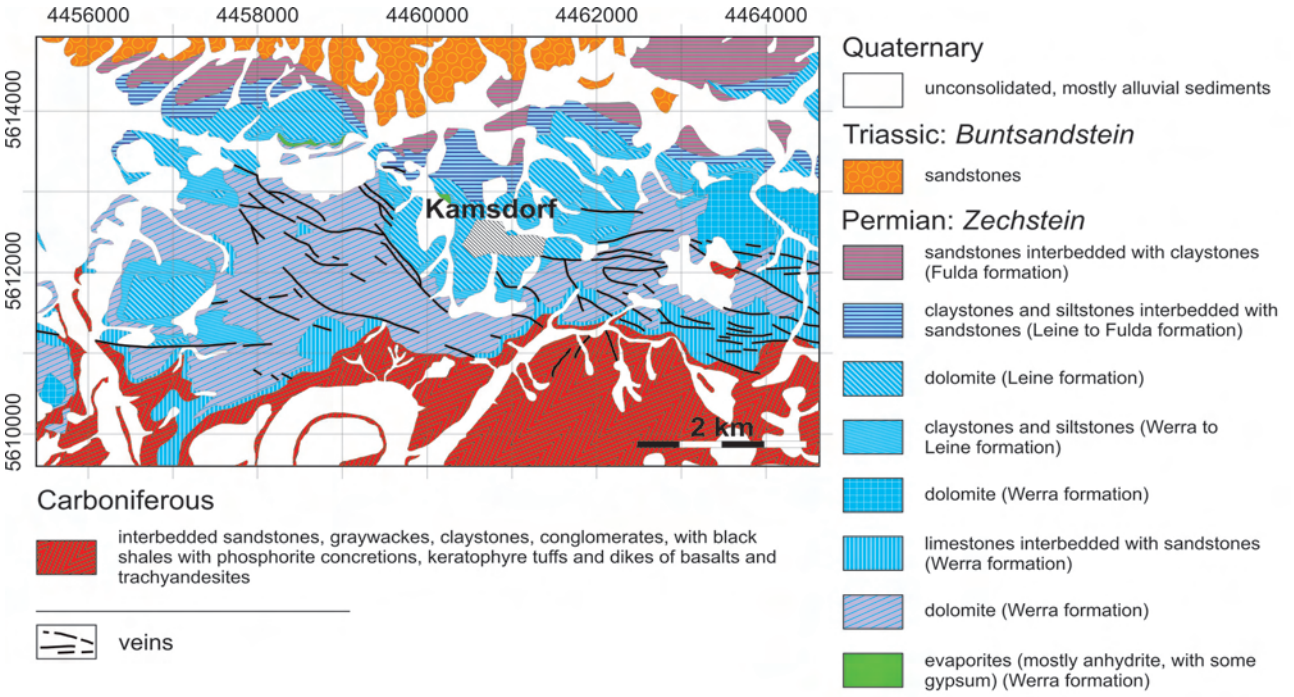

Fig. 2. Geological map of the vicinity of the village of Kamsdorf, with the barite-siderite veins (simplified after Wucher et al. 2001). The metasomatic siderite bodies are lying flat and do not appear on the geological map.

strike to the northeast (ENE 080) and show north-dipping and south-dipping thrust and reverse faults. Dip-slip striations perpendicular to the strike direction suggest an event of N–S compression.

In this study, we also analysed the direction of the mineralized fractures and veins. The main strike direction of the veins is to the northwest (Fig. 4 main direction of barite veins), which coincides with the direction of the extensional structures. In outcrops where veins and contractional structures intersect, a contractional overprint of the mineralizations is observable (Fig. 3).

Hence, a relative timing of the tectonic events and the mineralizations can be reconstructed in the available outcrops. The first event of NE–SW extension caused the formation of normal faults and extensional fractures. Afterwards, the hydrothermal fluids from the basement were injected into these fractures and deposited the observed mineralization. During the second deformation event, the vein mineralizations were deformed by small reverse faults and compressional fractures without mineralizations developed.

Gehren

The Ilmenau region (including the studied site Gehren) is located at the contact between the Thuringian Basin in the north, the Thüringer Schiefergebirge in the southeast and the Thüringer Wald in the southwest (Fig. 1). The exposed rocks, mostly of Neoproterozoic and Paleozoic age, were deformed and metamorphosed during the Variscan orogeny. Later deformation was mostly of brittle style and comprises several events of extension and contraction during the Mesozoic (Förster & Romer 2010). A detailed temporal reconstruction of the deformation and mineralization events was not possible within the framework of this work, due to the lack of well-exposed rocks in the studied area.

The only suitable exposures can be found in the underground of the adit Flußspatgrube in Gehren. There, the main fluorite-barite mineralization is spatially associated with a fault dipping towards the southwest (Franzke & Schiemenz 1980; Franzke et al. 1982; Franzke 1992). This normal fault shows an extensional character with tens of metres of displacement and is called the Floßberg fault. The Floßberg fault shows signs of polyphase activity during the Mesozoic, which is proved by K/Ar-dating of fault gouges and cataclastic rocks (Franzke et al. 1996). The development of the Floßberg fault began during the Middle Keuper (Karn; 228–225 Ma) and was possibly associated with a first episode of fluid migration into the fault zone. Afterwards, the fault zone was reactivated with normal senses of slip during Upper Jurassic (154–134 Ma) until Lower Cretaceous (123–102 Ma)

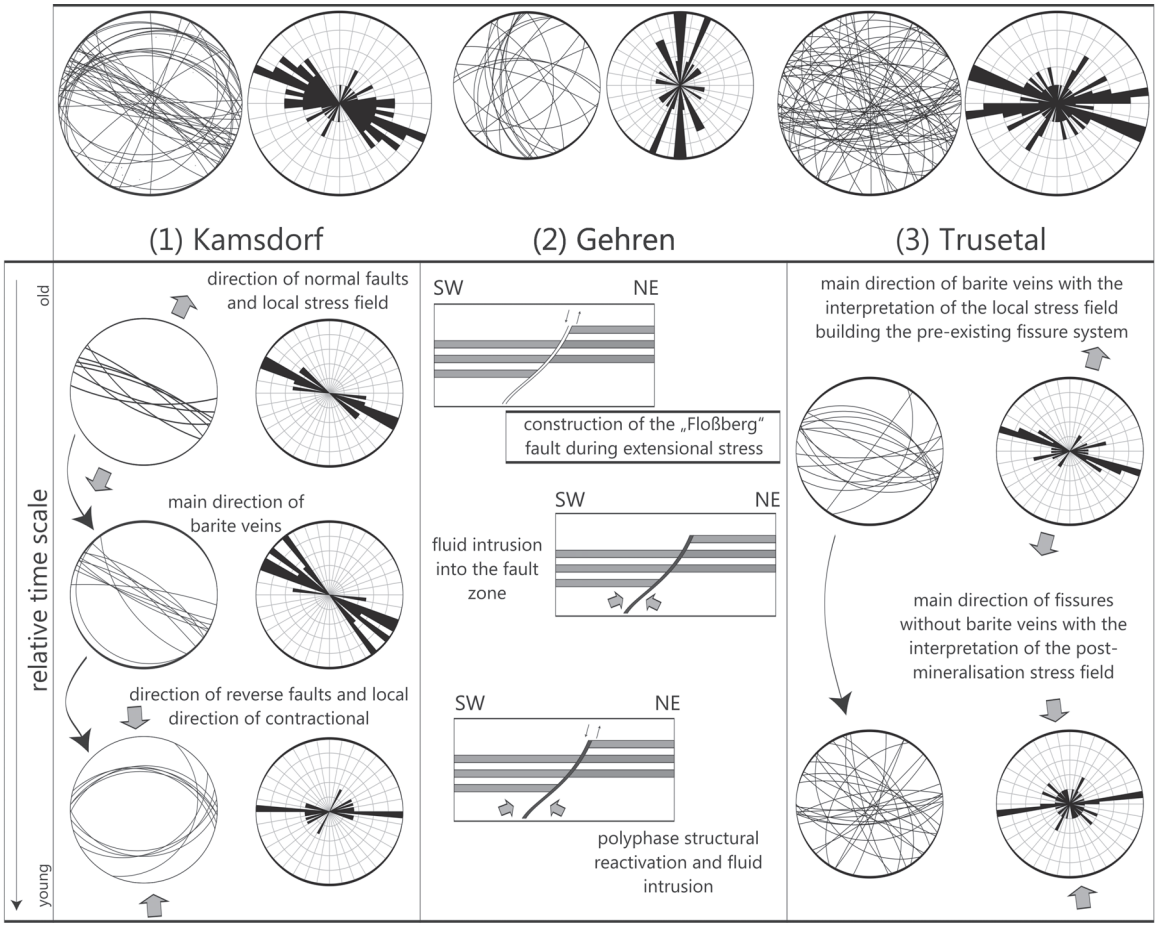

Fig. 4. Stereographic projections and rose diagrams of the structural measurements in Kamsdorf, Gehren, and Trusetal. If possible, the measurements are divided into different phases of formation.

times. Franzke et al. (1996) recognized several mineralization processes during these main deformation phases. A contractional reactivation of the Floßberg fault during the Late Cretaceous is not well documented in the outcrops but probably led to a compressional overprint of the mineralizations.

Trusetal/Hühn region

Trusetal is located at the border of the Thüringer Wald to its southern foreland (Fig. 1). The exposed rocks in this area are Variscan gneisses and granites of the Mid-German-Crystalline rise as well as *Zechstein* evaporites and Triassic rocks of the sedimentary cover. The deposit Hühn itself is located in the Variscan high-grade complex. Our strike and dip measurements of fissures can be divided into two main and one minor directions of brittle fractures. The main strike directions are oriented principally E–W and WNW–ESE (Fig. 4) and coincide with the direction of post-Variscan brittle deformation in the Kamsdorf and Ilmenau regions. The minor strike direction is NE–SW trending and agrees with the mean strike direction of the Variscan consolidated basement, thus probably indicating late syn-Variscan deformation. For illustration, fissures with and without barite veins were plotted separately (Fig. 4). An obvious conclusion drawn from Fig. 4 is that the barite veins mostly show the WNW–ESE direction. In contrast, barren fractures show the E–W direction. With the assumption that fluids only enter open fissures, the construction of WNW–ESE fractures must be described as the first deformation event. Afterwards, the influx of fluids predating the creation of E–W fractures led to the mineralization of pre-existing fissures of the first deformation event. Subsequent contraction resulted in the formation of E–W fractures without mineralizations and in the deformation of the rocks and veins. In the Hühn region, no absolute timing constraints can be found. Nevertheless, in relation to the wider area, the earliest time of deformation can be assumed to post-date Late Permian times due to NW–SE-striking barite veins within *Zechstein* sediments in the outcrops of the Hohe Klinge and the Grube Mommel. Accordingly, a polyphase deformation history can be assumed for the area around Trusetal. The dominant deformation characteristics are extensional. A compressional regime has prevailed in this area since the Late Cretaceous until the present time (Rauche & Franzke 1990).

Mineralogy and geochemistry

Siderite-barite-fluorite deposits

The mineralogy of these deposits is in most cases simple (Fig. 5). The major minerals are carbonates (calcite, ankerite, siderite), barite, and fluorite but they need not occur together in one deposit. Some deposits are missing fluorite, other ones siderite. Sulphides are found essentially only at the Kamsdorf deposit as lenses and disseminated mineralization in the siderite bodies or in the barite veins. In Kamsdorf, the *Zechstein* carbonate rocks which host the siderite bodies contain two thin (10–130 cm) horizons of grey shale enriched in pyrite. This shale occupies the same stratigraphic position as the *Kupferschiefer* shale and is considered to be an analogue of *Kupferschiefer*. A clear spatial relationship between the shales in Kamsdorf and the sparse sulphidic mineralization could not be proven, but also not refuted. The sulphides found in Kamsdorf are pyrite, chalcopyrite, marcasite, tennantite, tetrahedrite, and galena. The deepest accessible portions of the deposit also contain Co-Ni-As sulphides and Ag-rich tetrahedrite. The other studied barite-fluorite deposits contain very little or essentially no sulphides (for example Hühn, Pratzka 1956; Hähnel et al. 1995).

Mn-Fe deposits

The minerals reported in this section were identified by reflected-light polarized microscopy, powder X-ray diffraction, and electron microprobe. The analytical results of the electron microprobe studies are tabulated in Brey-Funke (2014). The bulk chemical composition of the Mn-Fe samples (determined by XRF, see Brey-Funke 2014), when placed in the discrimination diagram of Toth (1980), indicates hydrothermal origin of the studied ores. The mineralogy of the two districts with Mn-Fe mineralizations (Arlesberg and Oehrenstock, both in the vicinity of Ilmenau, Fig. 1) is different. At Arlesberg, the veins and nests hosted by rhyolites (Figs. 6, 7a) contain hematite, braunite, pyrolusite, barite, and traces of manganite. Only small and insignificant veins were emplaced in the conglomerates of the *Rotliegend* (Fig. 6, Brosin & Veitenhansl 2005). At Oehrenstock, the mineralized structures located in the acidic pyroclastic rocks contain hausmannite, manganite, braunite, barite, and several varieties of calcite.

In the samples from Arlesberg which contain both hematite and Mn minerals, coarse-grained, crystalline hematite is the earlier mineral. In addition, hematite and the Mn minerals are usually spatially separated, hematite occupying deeper portions of the deposit (Beyschlag 1914). Historical accounts report that manganite was common at Arlesberg but Schiemenz (2001) notes that manganite cannot be found there today. We have not found manganite at Arlesberg either and the historical accounts should be perhaps taken with a grain of scepticism. Braunite, on the other hand, is abundant at Arlesberg. It replaces the rock-forming minerals

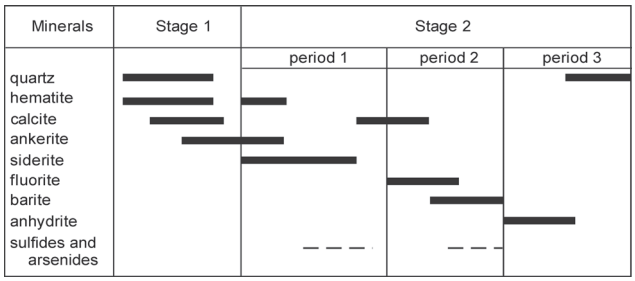

Fig. 5. Sequence of the vein mineralisations of the barite-fluorite-siderite mineralization at the southern edge of the Thuringian Basin (based on our observations and the reported temporal relationships from Pratzka, 1956; Werner, 1958; Kuschka & Franzke, 1974; Meinel, 1993; Hähnel, et al. 1995; Kling, 1995; Kießling, 2007).

of the rhyolite, first the feldspars in the fine-grained matrix of the volcanic rock, then the K-feldspars, and eventually also quartz in the matrix. Occasionally, the rims of the braunite grains are replaced by pyrolusite. Pyrolusite also forms pseudomorphs after manganite; the earlier manganite was observed very rarely (Fig. 7f). The abundance of the pseudomorphs could be also the explanation for the early descriptions of manganite from Arlesberg.

In the samples from Oehrenstock, the mineralization commences with hausmannite, mostly as massive aggregates, rarely as subhedral crystals with mosaic texture. Manganite is found as prismatic or acicular crystals and, according to our observations in polarized light, is slightly younger than hausmannite. Hausmannite is replaced to a great extent by euhedral to subhedral crystals of braunite. The crystals are porous and the cores of the crystals are replaced by calcite, less commonly by barite (Figs. 7d,e). Calcite, as mentioned, occurs here in several varieties or perhaps generations. The earliest variety is black calcite, macroscopically similar to the Mn oxides (Fig. 7b). In an optical microscope and back-scattered electron images, one can see innumerable microscopic inclusions of Mn oxides in the calcite (Fig. 7c), responsible for its black colour. The analysed inclusions appear to have already weathered to hollandite and cryptomelane. Black calcite replaces manganite, according to Schiemenz (2001) also hausmannite and braunite. Younger, brown calcite replaces braunite and black calcite. The youngest variety is coarse-crystalline, sometimes euhedral white calcite.

Barite is a relatively young mineral within the precipitation sequence. Locally, however, crystals of manganese crystals clearly grow on the aggregates of barite. These features may be a result of multiple remobilization of manganese or multiple generations of barite.

Late stage evolution of the deposit are marked by cryptocrystalline hematite, braunite, and calcite. Weathering minerals include hollandite, cryptomelane, coronadite, todorokite, chalcophanite, and romanèchite.

Comparison of the size of the two types of deposits

For the later discussion of geological and geochemical similarities of the studied mineralizations, it is of interest to compare their size and ore resources. The extracted 44,700 tonnes of manganese ores in the Arlesberg (F. Veitenhansl, pers. comm.) district are dwarfed by the 1.4 million tonnes

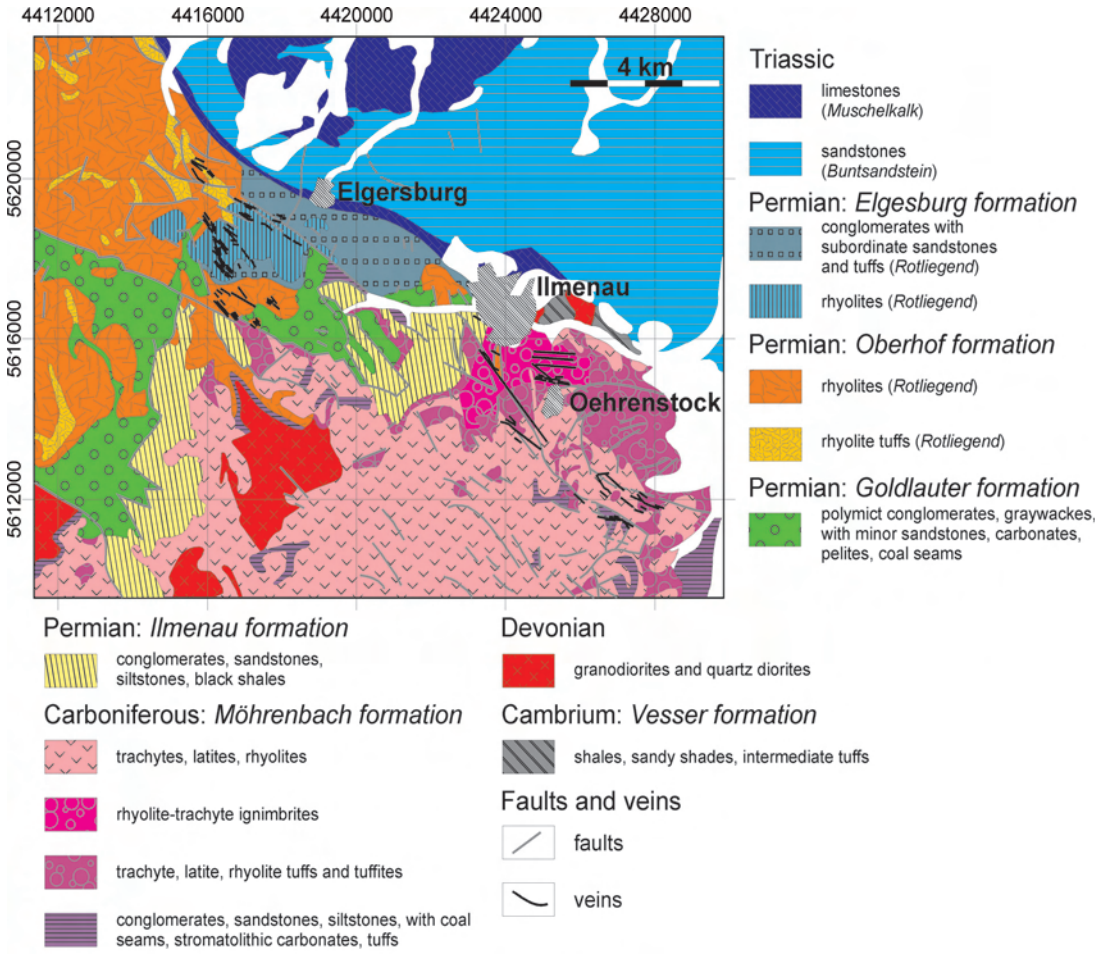

Fig. 6. Geological map of the vicinity of the township of Ilmenau, with the Mn-Fe ores veins. Note the close spatial association of these veins and the Permian volcanic rocks (geological map simplified after Andreas et al. 1996).

siderite from Kamsdorf. Are the historical manganese districts really just mineralogical occurrences? Below, we assume that the two Fe-Mn assemblages (siderite+ankerite *versus* Mn oxides-silicates) have much more in common than meets the eye. Using the measured chemical composition of siderite (see Brey-Funke 2014 for the analyses), we can calculate the amount of siderite that would comprise 44,700 tonnes of manganese ores. Taking the mineralogy of the Mn ores into account (relative proportions of the oxides and silicates), it can be estimated that 1.0–1.3 million tonnes of siderite would be needed. This amount compares very well with the 1.4 million tonnes extracted at Kamsdorf and suggests that, at least in terms of their size, the deposits could be very similar.

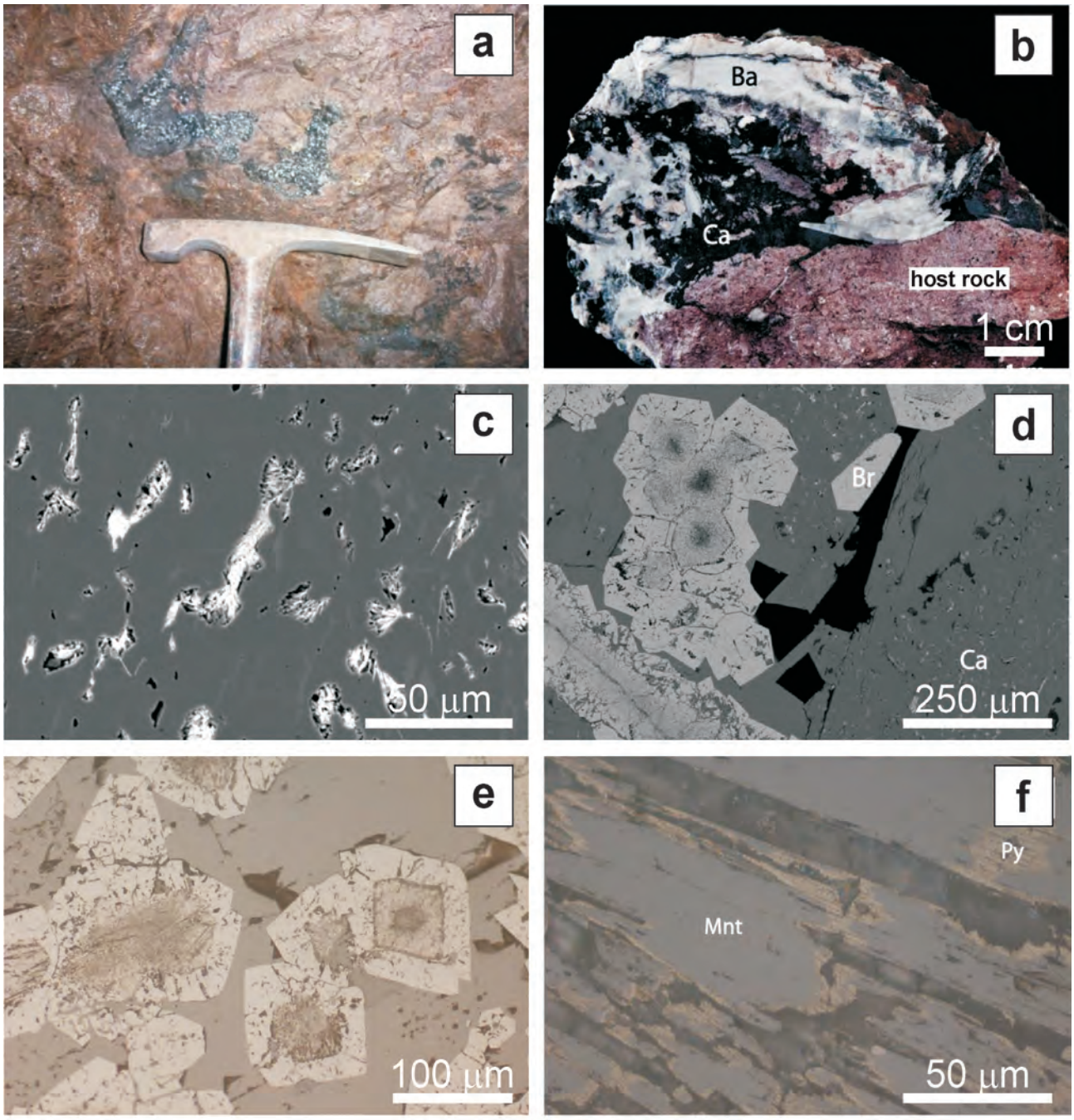

Fig. 7. a — Nests of pyrolusite in rhyolite near Arlesberg. Note that minerals other than pyrolusite are missing in these nests; **b** — a portion of a hydrothermal vein with barite (Ba) and black calcite (Ca) (Oehrenstock, the dump Willhelm Glück); **c** — back-scattered electron (BSE) image of the black calcite, showing the calcite (grey) matrix and inclusions of Mn oxides (white); **d,e** — aggregates of braunite (Br) crystals in calcite. Note that the cores of braunite crystals are selectively replaced by calcite (**d** — BSE image, **e** — reflected-light image); **f** — reflected-light microphotograph of rare manganite (Mnt) crystals, replaced from the rims and along the cracks by pyrolusite (Py).

Fluid inclusion petrography and microthermometry

Fluid inclusions were analysed in siderite, calcite, fluorite, and barite. No fluid inclusions were found in the bluish, massive anhydrite. Emphasis was placed on studying primary fluid inclusions, even though secondary inclusions were commonly observed. We characterized an inclusion as primary according to the criteria listed in Roedder (1984) after a careful petrographic study of the sections.

Siderite, calcite, fluorite

Fluid inclusions in siderite, calcite and fluorite (Fig. 8) contain either a two (aqueous liquid and water vapour) or a single (aqueous) phase. Most of the inclusions are irregular but negative crystal shapes were also observed, particularly in fluorite, less commonly in the carbonates. The liquid:vapour ratio in the two-phase inclusions was consistently approximately 90:10. The size of the primary inclusions varies between 5 and 100 μm. The secondary inclusions are smaller, with sizes from <5 to 20 μm, arranged in trails, and often consisting of a single aqueous phase.

The primary fluid inclusions from siderite, calcite, and fluorite show a range of T_e values from –65.6 to –49.7 ˚C (Table1), indicating predominantly the H_2O-NaCl-$CaCl_2$ system in the aqueous phase (Davis et al. 1990; Spencer et al. 1990). Final melting temperatures of ice ($T_{m,ice}$) range from –36.6 to –25.2 ˚C. The salinities of the included fluids vary in a narrow range and are graphically shown in Fig. 9. To facilitate comparison among all measured inclusions, all data are presented in eq. mass % $CaCl_2$. Melting of hydrohalite was observed only in four fluorite samples from *Gehren*, *Ilmenau*, and *Hühn* (Table 1). In those fluid inclusions, where melting temperatures of both ice and hydrohalite were measured, the fluid compositions were derived using the approach of Steele-MacInnis et al. (2011). The resulting calculated $CaCl_2/(CaCl_2+NaCl)$ ratios are in the range of 0.4 to 0.6 (Fig. 10).

The fluid inclusions in siderite, calcite, and fluorite always homogenize to the liquid phase, with T_h values between 134 to 163 ˚C for siderite and 103 and 134 ˚C for calcite (Fig. 9, Table 1). The inclusions in fluorite have homogenization temperatures of 73–127 ˚C for samples from *Gehren*; 81–135 ˚C for *Ilmenau* (*Volle Rose*); 65–129 ˚C for the *Hühn* region and 69–141 ˚C for *Eisenach-East*.

Barite

Barite samples from all the studied deposits are similar in terms of the observed fluid inclusions and their composition. Based on the number of phases present at room temperature, the fluid inclusions in barite can be divided into four groups: 1. two-phase liquid-rich, 2. two-phase vapour-rich, 3. one-phase with only a liquid phase and 4. one-phase with only a vapour phase. All types can be found together in close vicinity with each other. Group 1 inclusions generally show a liquid to vapour ratio of 85:15. We suppose that fluid inclusions with the predominant gas phase or only with the gas phase are a result of leakage coincidental with the post-mineralization tectonic events.

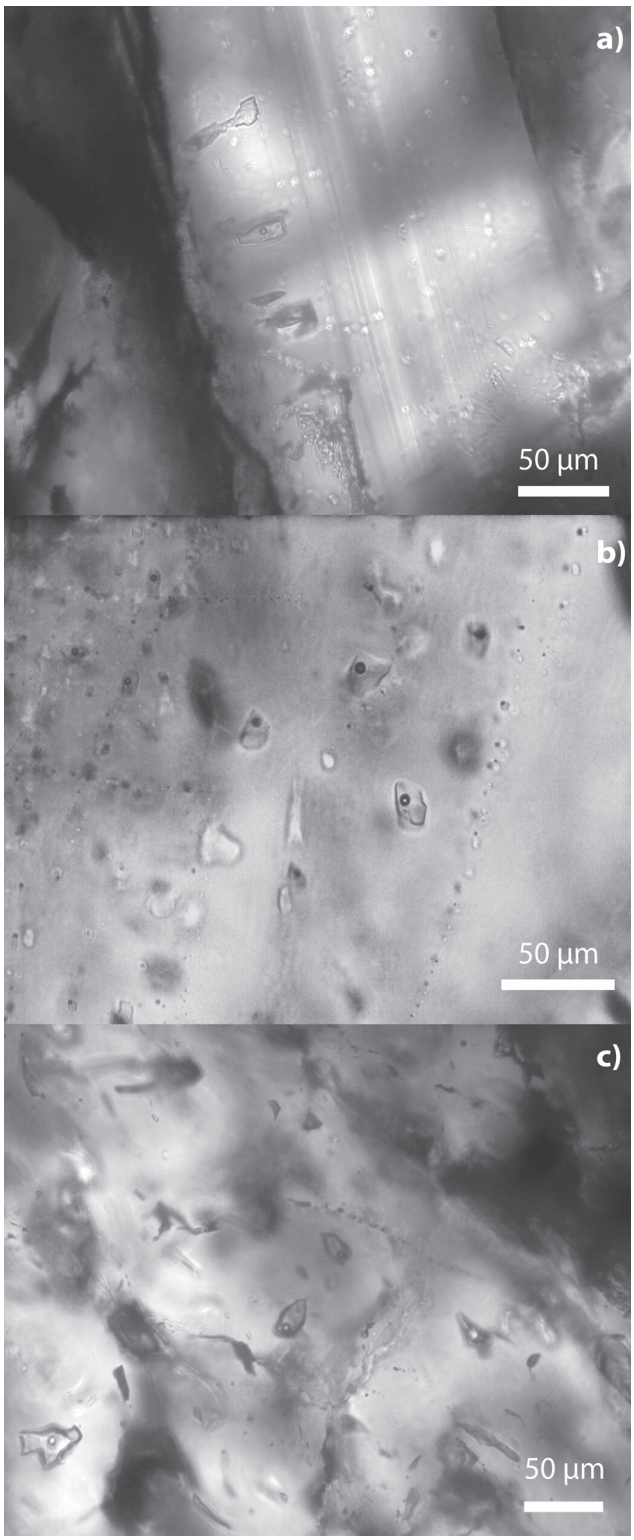

Fig. 8. Microphotographs of fluid inclusions in the studied mineralizations. **a** — two-phase primary fluid inclusion in siderite; **b** and **c** — primary and secondary fluid inclusions in fluorite and barite, respectively.

Table 1: Microthermometric data for primary fluid inclusions in barite, fluorite, calcite, and siderite. All temperatures in ˚C.

Region	Sample	Mineral	T_e (n)	$T_{m,ice}$ (n)	$T_{m,hydrohalite}$ (n)	T_h (n)
	KAM 1	barite	–53.0 to –42.8 (4)	–23.8 to –17.6 (4)	NM	156 (1)
Saalfeld -	KAM 2	barite	–36.9 to –25.3 (2)	–25.4 to –14.4 (2)	NM	NM
Kamsdorf	KAM 7b	barite	–46.2 to –30.1 (3)	–21.0 to –12.0 (6)	NM	116 to 160 (4)
	KAM 9	barite	–50.1 to –25.0 (2)	–24.0 to –12.6 (3)	NM	158 (1)
	KAM 11	barite	–53.9 to –51.3 (2)	–25.3 to –9.4 (3)	–21.5	NM
	KAM 14	barite	–50.9 to –50.1 (3)	–20.2 to –17.1 (3)	NM	156 (1)
	KAM 15	barite	–51.1 to –24.3 (3)	–15.1 to –11.4 (3)	NM	107 (1)
	HG 25330	barite	–52.6 to –49.4 (5)	–26.8 to –18.4 (9)	NM	87 to 120 (5)
Friedrichsroda	HG 25312	barite	–52.3 to –48.3 (4)	–26.3 to –17.7 (6)	NM	91 to 161 (4)
	GEH 2	calcite	–61.3 to –54.3 (5)	–33.0 to –27.4 (12)	NM	103 to 134 (12)
Gehren	GEH 2	fluorite	–55.7 to –53.3 (2)	–32.0 to –31.2 (3)	NM	94 to 127 (4)
	GEH 3	barite	–52.6 to –48.9 (4)	–24.0 to –17.9 (8)	NM	104 to 107 (5)
	GEH 3	fluorite	–61.3 to –52.9 (9)	–38.0 to –27.0 (20)	NM	75 to 127 (20)
	GEH 5	fluorite	–61.3 to –53.8 (7)	–36.2 to –29.3 (15)	NM	73 to 123 (15)
	GEH 7	fluorite	–60.9 to –52.3 (6)	–35.2 to –27.6 (15)	–10.8 (1)	99 to 121 (7)
Volle Rose	VR 1	fluorite	–69.3 to –49.7 (6)	–35.8 to –25.2 (17)	–9.7 to –8.8 (3)	81 to 135 (15)
(Ilmenau)	BHÜB 1	barite	–51.3 to –49.0 (3)	–25.6 to –18 (4)	NM	128 to 161 (2)
Hühn - Trusetal	HÜB 4	fluorite	–61.4 to –58.0 (6)	–38.8 to –27.9 (18)	–15.9 to –5.3 (3)	65 to 129 (18)
	HÜB 6	barite	–50.9 to –49.2 (4)	–22.7 to –21.0 (10)	NM	67 to 124 (9)
	HÜB 6	fluorite	–63.6 to –63.4 (5)	–35.3 to –25.2 (10)	–7.6 (1)	70 to 129 (21)
	SID 1	siderite	–52.9 to –50.5 (6)	–36.6 to –27.4 (18)	NM	134 to 163 (15)
Eisenach - East	EO-I-4997	fluorite	–65.6 to –61.4 (2)	–37.3 to –26.4 (17)	NM	69 to 141 (16)
	EO-102	barite	–51.4 to –48.8 (3)	–24.1 to –13.9 (10)	NM	97 to 166 (6)
Oehrenstock	EGS 10a	calcite	–51.7 to –47.3 (10)	–26.2 to –23.4 (15)	NM	89 to 140 (21)
	EGS 10c	calcite	–55.0 to –48.0 (11)	–31.2 to –21.8 (16)	NM	78 to 168 (20)
	EGS 7i	barite	–67.0 to –48.2 (12)	–39.6 to –21.6 (15)	NM	101 to 156 (17)
Arlesberg	EGS 17c	barite	–60.2 to –49.4 (9)	–41.9 to –23.1 (15)	NM	78 to 149 (15)

T_e — eutectic temperature
$T_{m,ice}$ — melting temperature of ice
$T_{m,hydrohalite}$ — melting temperature of hydrohalite
T_h — total homogenisation temperature
n — number of measurements
NM — not measured

The primary inclusions occur as isolated and three dimensional clusters (Fig. 8c), with their size ranging from 10 μm to 350 μm. Most of them are irregularly shaped; some are rounded or elongated. Primary fluid inclusions with a negative crystal shape are rare and were found only in a few cases. Primary inclusions are liquid-rich with a gas bubble. The secondary inclusions occur along trails and are of very small size <5 μm to 10 μm. Most of the secondary trails contain rounded and irregular fluid inclusions, with single gas phase.

For fluid inclusions study in barite, a further selection was carried out for the inclusions to be measured. The inclusions were carefully selected according to the criteria of Ullrich & Bodnar (1987): they were small, with round shape and smooth walls. According to Ullrich & Bodnar (1987) such inclusions in barite are most likely to yield correct data and withstand post-depositional damage, mostly owing to the excellent cleavage of barite. Even data for inclusions with no signs of leakage, necking down and so on were discarded if they were larger or elongated. The measured T_h values are reproducible, suggesting that the measured inclusions are not prone to leakage at the present time. Additionally, we have tested the validity of the fluid inclusion data in a double-sided polished section that consisted of barite with millimetre-thick bands of fluorite. The results are shown in Fig. 9d, documenting the accuracy of the information from the inclusions in barite. Further support for the validity of the fluid inclusion data for barite comes from the measurements in co-existing barite and calcite from the Fe-Mn mineralization (Fig. 9c). Here, the scatter for the data in both minerals is identical, documenting that the fluid inclusions in barite yield correct and useful data.

Primary fluid inclusions in barite from the *Kamsdorf-Saalfeld* region record a broad range of $T_{m,ice}$ and T_h temperatures (Fig. 9b). The measured T_e in all these barite samples varies from –53.9 to –24.3 ˚C (Table 1), with most values in the range around –50 ˚C, typical for systems with an appreciable concentration of $CaCl_2$ (Hurai et al. 2015). Values of $T_{m,ice}$ range between –23.8 to –9.4 ˚C with corresponding salinities of 22.3 to 13.6 eq. mass % $CaCl_2$. The homogenization temperatures in these samples range between 116 and 160 ˚C. Individual barite samples from all studied locations, that is, *Friedrichsroda*, *Gehren*, *Hühn* and *Eisenach-East* show a similar scatter of results (Table 1, Fig. 9b).

The fluid inclusions from *Oehrenstock* and *Arlesberg* (the Fe-Mn mineralization) also point at the system H_2O-NaCl-$CaCl_2$ with their T_e temperatures of –67.0 to –48.2 ˚C. The ice melting temperatures of –41.9 to –21.6 ˚C, correspond to salinities of 28.5 to 21.3 wt % $CaCl_2$ eq. The T_h values ranged between 78 and 156 ˚C.

Stable isotope data

The results of the $\delta^{34}S$ and $\delta^{18}O$ stable isotope analyses from a suite of barite and one anhydrite sample are given in

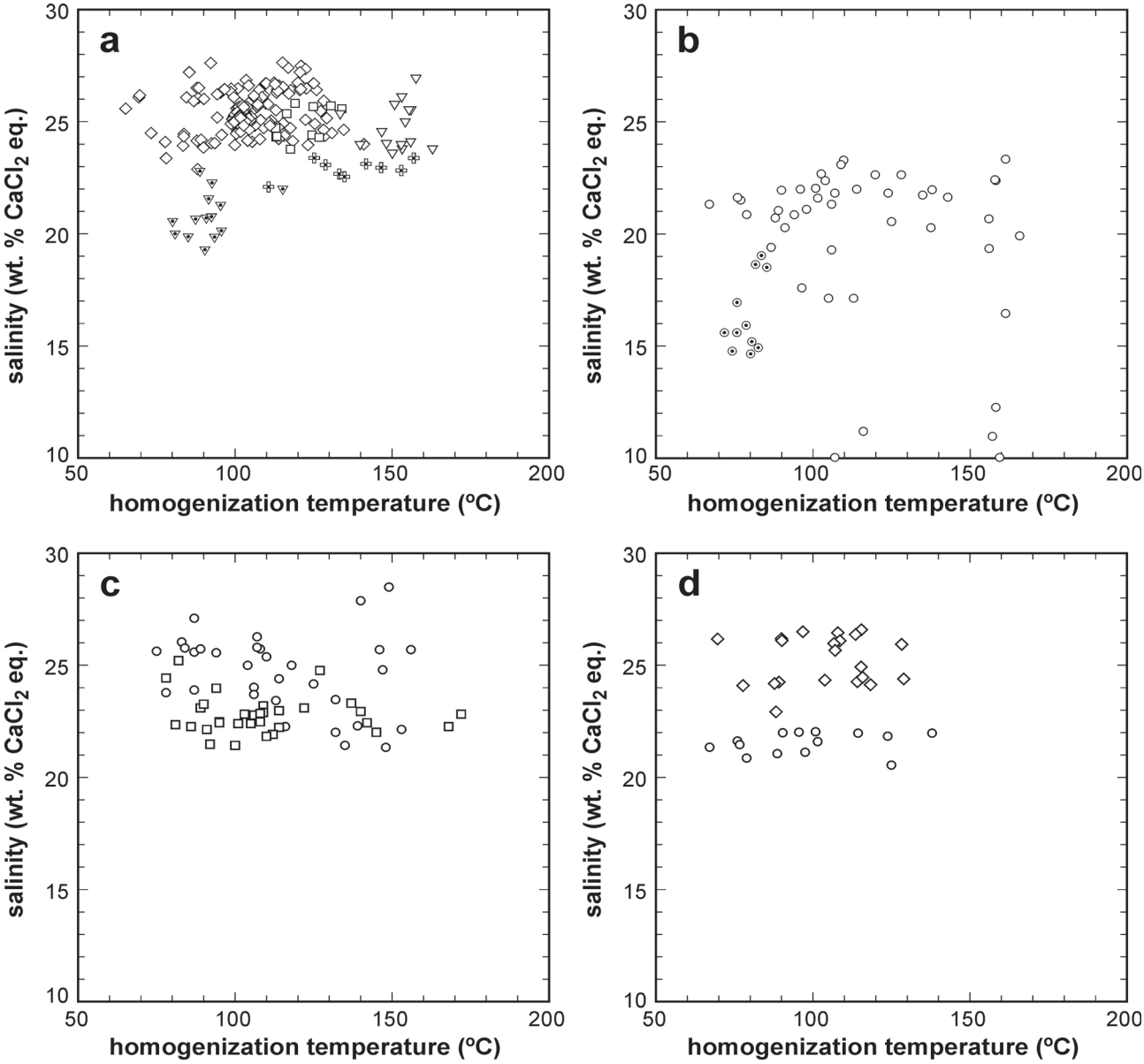

Fig. 9. Homogenization temperatures and salinities of fluid inclusions in the studied mineralizations. Data for fluid inclusions in: **a** — siderite (triangles), fluorite (diamonds), calcite (squares), and ankerite (crosses) from the barite-fluorite-siderite mineralization. The symbols with a dot in the centre represent data from Kling (1995); **b** — barite from the barite-fluorite-siderite mineralization. The symbols with a dot in the centre represent data from Kling (1995); **c** — calcite (squares) and barite (circles) from the Mn-Fe mineralization; **d** — fluorite (diamonds) and barite (circles) from a single double-sided polished section from Hühn.

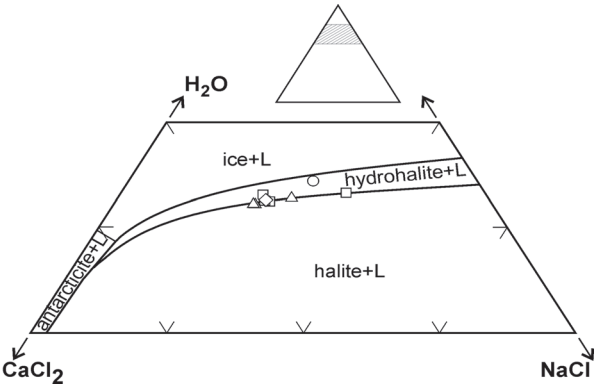

Fig. 10. Ternary plot of phase relations in the H_2O-NaCl-$CaCl_2$ system, with the composition of the studied fluid inclusions calculated by the methodology of Steele-MacInnies et al. (2011). The solid lines represent cotectic curves that separate the stability fields of ice, halite, hydrohalite, and antarcticite. Shown are NaCl/(NaCl+$CaCl_2$) weight fractions for fluid inclusions obtained from final hydrohalite melting temperatures. Calculated NaCl/$CaCl_2$ ratios in individual fluid inclusions in fluorite (squares=Hühn/Trusetal; triangles=Ilmenau; diamond=Gehren) and barite (circle=Kamsdorf).

Table 2 and plotted in Fig. 11. The results from this study compare well to the previously reported values of Lahiry (1974). Variations between barite-bearing veins hosted by different lithological units, like the crystalline basement, Permian rhyolite and *Zechstein* dolomite are relatively small but there are systematic variations. It seems that the barite samples hosted by the volcanic rocks (rhyolites, acid volcanoclastic rocks) have lower $\delta^{34}S$ values than the other samples, with one exception. Fig. 11 also shows a comparison with sulphate minerals (barite and anhydrite) from the North German basin. Although this basin is now separated from the Thuringian basin by the crystalline complex of the Harz Mountains, the two basins represented a single sedimentation space in the Permian. Therefore, the results from the North German basin can be used for the comparison with our data.

Table 2: Sulphur and oxygen isotopic data of hydrothermal barite and anhydrite hosted in crystalline basement, *Rotliegend* sediments and *Zechstein* sedimentary rocks.

Sample	Locality	Host rock	$\delta^{34}S_{V\text{-}CDT}$ (‰)	$\delta^{18}O_{V\text{-}SMOW}$ (‰)
barite in the siderite-barite-fluorite mineralization				
KAM 9	Kamsdorf	*Zechstein* sedimentary rocks	13.6	14.8
KAM 11	Kamsdorf	*Zechstein* sedimentary rocks	14.0	14.7
KAM 15	Kamsdorf	*Zechstein* sedimentary rocks	12.8	13.9
Geh 3	Gehren	*Rotliegend* volcanics and sediments	9.3	12.2
HG 25312	Friedrichsroda	*Rotliegend* volcanics and sediments	15.4	13.1
Hüb 6	Trusetal	crystalline basement	12.2	12.4
Bhüb 1	Trusetal	crystalline basement	13.2	12.7
barite in the Mn-Fe mineralization				
EgS8b	Öhrenstock	Permian volcanoclastic rocks	9.9	14.6
EgS9c	Öhrenstock	Permian volcanoclastic rocks	9.5	9.1
EgS17c	Arlesberg	Permian rhyolites	8.7	12.2
EgS17g	Arlesberg	Permian rhyolites	7.9	13.1
anhydrite				
Hühn 1	Trusetal	crystalline basement	10.4	12.1

Isotopic analyses of carbonates from the studied veins ($\delta^{13}C$ and $\delta^{8}O$ values) are summarized in Table 3 and plotted in Fig. 12, together with isotopic composition of carbonates from hydrothermal veins in Schwarzwald (Schwinn et al. 2006) and cement, fissure filling and druses of carbonates from the North German basin (Wolfgramm 2002). The materials analysed from the North German basin came mostly from Permian rocks (siliclastic and volcanic rocks), with a few samples from Upper Carboniferous and Mesozoic rocks. Similar rocks also occur in the Thuringian basin.

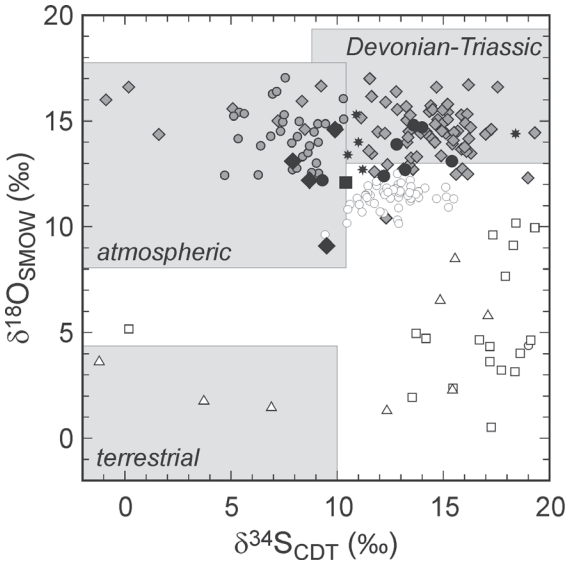

Fig.11. Isotopic composition of barite from the barite-fluorite-siderite mineralization (black circles, this study), barite from the Mn-Fe mineralization (black diamonds, this study), anhydrite from the anhydrite veins (black square, this study), barite from the mineralizations in the Thuringian basin (black stars, Lahiry 1974), anhydrite in the Zechstein rocks in western Poland (open circles, Peryt et al. 2010), anhydrite in the Rotliegend rocks from the Northeast German basin (open squares, Wolfgramm 2002), anhydrite and barite from Permian volcanic rocks from the Northeast German basin (open triangles, Wolfgramm 2002), hydrothermal sulphates in the Middle Harz Mountains (grey circles, Zheng & Hoefs 1993), and hydrothermal sulphates in the Upper Harz Mountains (grey diamonds, Zheng & Hoefs 1993). The fields of Devonian-Triassic, atmospheric, and terrestrial sulphates after Clark & Fritz (1997) are also shown. Note that these fields are cut off according to the spread of the data points and actually extend beyond the limits of this diagram.

Discussion

Fluid evolution

Fluid inclusion studies in siderite, calcite, and fluorite show a narrow range in salinity (22.9 to 27.7 eq. mass % $CaCl_2$) and homogenization temperatures between 134 and 163 ˚C for siderite and between 65 and 135 ˚C for calcite and fluorite (Fig. 9). These results are in good agreement with previous fluid inclusion studies of fluorite veins in Ilmenau & Trusetal (Hühn) area (Lahiry 1974; Thomas, 1979; Loos et al. 1981; Klemm, 1986; Hähnel et al. 1995). Fluid inclusion studies of barite samples from the Thüringer Wald and the Kamsdorf area show a greater scatter of salinities between 13.6 and 26.8 eq. mass % $CaCl_2$, also documented by Meinel (1993) and Thomas (1979). In line with our results, studies have reported homogenization temperatures of about 50 ˚C in barite samples from the Thüringer Wald (Thomas 1979; Hähnel et al. 1995) and 80 ˚C for barite from Kamsdorf region (Kling 1995). In our work, we have measured a wide spread of homogenization temperatures between 65 to 166 ˚C in all barite samples (Fig. 9). Hence, we observe a monotonous decrease of the fluid temperatures from

134–163 ˚C to about 70 ˚C with constant salinity, only locally modified by mixing with low-salinity fluids during precipitation of the latest mineral, namely barite. The fluids responsible for the precipitation of siderite, calcite, fluorite, and barite were $CaCl_2$-NaCl brines (Table 1). In terms of composition and temperature, we know little about the fluids that deposited the Mn mineralization. The data presented here were measured in calcite and barite which accompany the Mn minerals but not in the Mn minerals themselves. Our attempts to observe fluid inclusions in the Mn minerals with infrared microscopy failed.

The $\delta^{34}S$ values of our barite samples vary between 9.3 and 15.4 ‰, a range typical of Upper Permian (*Zechstein*) and Triassic evaporitic rocks (Fig. 11), which fall between 9.7 and 12.6 ‰ in the *Zechstein* evaporites and 12.2 to 20.8 ‰ in the Triassic evaporites (Kramm & Wedepohl 1991; Kampschulte et al. 1998). Hence, most of the dissolved sulphate in the hydrothermal fluids was derived from groundwater and/or seawater that had interacted with the evapo-rites (Wagner et al. 2010). Barite with more positive $\delta^{34}S$ values than the average *Zechstein* sulphates could be explained by a contribution of sulphates from Triassic evaporites.

The isotopic composition of the fluids (for $\delta^{18}O$ relative to V-SMOW), calculated (after Zheng 1999) from the isotopic composition of the minerals and the homogenization temperatures of fluid inclusions, is 4.3 to 13.5 ‰ for calcite and 10.8 to 5.6 ‰ for barite. These values suggest that barite and calcite could not have precipitated from the same fluid. The isotopic composition of the fluid that precipitated barite is close to the sea water in the entire Permo-Mesozoic time span whereas calcite is isotopically distinctly heavier, as if the fluids were affected by evaporation. Further work is needed in order to interpret the isotopic data with more confidence.

Table 3: Carbon and oxygen isotopic data of hydrothermal carbonates from Öhrenstock. These veins are hosted by Permian volcanic rocks.

sample	description (cc=calcite)	$\delta^{13}C_{V\text{-}PDB}$ (‰)	$\delta^{18}O_{V\text{-}SMOW}$ (‰)
EGS 7h	black cc	–7.2	21.8
EGS 7o	black and white cc	–4.6	22.6
EGS 8a	black cc	–7.9	21.9
EGS 8d	white cc	–3.8	27.8
EGS 8g	white cc	–3.8	26.9
EGS 10b	white cc	–5.1	25.6
EGS 10b	black cc	–3.8	26.3
EGS 10c	white cc	–2.5	27.1

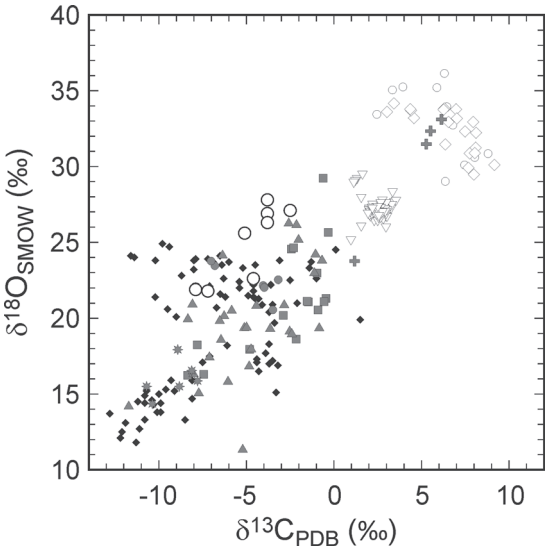

Fig. 12. Isotopic composition of the carbonates from the studied mineralizations (large open circles), compared to Triassic limestones (*Muschelkalk*, inverted open triangles, Lippmann et al. 2005), *Zechstein* calcite (west Poland, small open circles, Peryt et al. 2010), *Zechstein* dolomite (west Poland, open diamonds, Peryt et al. 2010), and hydrothermal mineralizations from Schwarzwald (small black diamonds, Schwinn et al. 2006). Furthermore showing the data from the Northeast German basin (all data from Wolfgramm 2002): Mesozoic rocks (grey circles), *Rotliegend* (grey squares), Permian volcanic rocks (grey triangles), *Zechstein* (grey crosses), Carboniferous rocks (grey stars)

Relative timing of the observed mineralizations

Within the mineralizations studied in this work, the relative timing is relatively easy to establish. We observed two distinct assemblages with sequences:

1. *siderite+ankerite-calcite-fluorite-barite*
2. *hematite-hausmannite-manganite-braunite-pyrolusite-calcite-barite.*

Here we neglect the minor sulphides and products of weathering. There are several observations which will be critical for the following discussion. First, the geochemistry of the earlier stages of both assemblages (*siderite+ankerite*) versus (*hematite-hausmannite-manganite-braunite-pyrolusite*) is very similar and we consider these earlier stages of the two assemblages to be coeval. These stages are both Mn-Fe rich. Siderite and ankerite are restricted mostly to metasomatic bodies in the Upper Permian *Zechstein* rocks, the oxide and silicate Mn-Fe minerals to the Permian volcanic or volcanoclastic rocks (Fig. 6). In the case of the Mn-Fe oxide-silicate assemblage, we see spatial separation of the Fe-rich portions (dominated by hematite) and Mn-rich portions (dominated by Mn oxides and braunite). This observation suggests that both metals (Fe and Mn) were originally reduced in the fluid and then separated by redox gradients.

The second interesting observation is that barite is relatively young in both mineralizations. In hand specimens, barite and Mn minerals are intergrown and barite seems to be both older and younger than some Mn minerals. This observation indicates either remobilization of Mn minerals during deposition of barite or multiple barite generations. Fluid inclusion and isotopic data suggest that the fluids responsible for barite in both assemblages were very similar.

Post-Variscan evolution of fluids in the Thuringian Basin

The post-Variscan fluids and the associated mineralizations in the Thuringian Basin can be correlated with the processes which operated in the thick Permian siliciclastic sequence

called *Rotliegend* (Fig. 13a). The properties of the fluids which co-existed with these sediments throughout post-Variscan Europe in the geological past were determined by the investigation of the mineralogical and geochemical changes in these sediments (Gaupp & Okkerman 2011) (Fig. 13a). The information about these fluids, reported below, draws on their publication. A temperature profile through the geological time of a selected Permian stratum (*Kupferschiefer*) in the area studied is presented in Fig. 13d. We must stress that our work investigated neither the *Rotliegend* sediments nor their evolution in space, time, and chemical composition (including that of the fluids). We correlate the data from these sediments, acquired over a long time by R. Gaupp and his co-workers, with our results from the vein mineralizations in the area studied. Hence, the physico-chemical properties of the fluids and the mineralogy of the siliciclastic sediments, described in the following paragraphs, refer to the fluids in the *Rotliegend* (Gaupp & Okkerman 2011), unless stated otherwise.

Stage 1. Early diagenetic post-Variscan fluids were playa-sediment fluids which circulated in the freshly deposited siliciclastic sediments of *Rotliegend*. These fluids were alkaline and saturated with respect to sodium sulphate, carbonate, and chloride. The anion abundance also decreased in the same order. The evidence for this character of the fluid comes from the absence of feldspar alteration during the early diagenesis. We assume that the alkaline nature of the fluids enabled them to mobilize quartz in amounts that were larger than in the later fluids. Evidence for mobilization of SiO_2 is also traceable on the microscale as quartz overgrowths on the detritic quartz grains in the sediments. Hence, these fluids were at least initially oxidizing and precipitated quartz, calcite+hematite instead of siderite.

Stage 2. The pH of the fluids in this stage has shifted to mildly acidic. The acidification of the fluids was caused by the release of carboxylic acids from the organic matter (cf. Spirakis & Heyl 1988) released from the Westphalian carbonaceous sediments. The redox state shifted to reducing, as clearly indicated by pervasive chloritization and deposition of the Fe^{2+}-bearing carbonates within the pore spaces of the siliciclastic rocks. The mildly acidic and reducing conditions are ideal for the mobilization of iron and manganese, possibly other metals and metalloids, from the *Rotliegend*. This mobilization is documented by bleaching of the sediments (Fig. 13a) upon which they lost their typical red colour and turned beige or almost white. In this process, hematite, other metal oxides and the elements associated with these mine-rals were dissolved in the pore fluids. We further subdivide this stage into two parts but we want to emphasize that these two substages (2A and 2B) are not separated in time. Instead, they are separated by different physico-chemical conditions of mineral precipitation.

Substage 2A. Where these fluids invaded the *Zechstein* carbonates, they deposited the assemblage siderite+ankerite in the form of metasomatic bodies and veins. Deposition of the Fe^{2+}-bearing carbonates in the pores of the siliciclastic sediments means that the fluids were saturated or supersaturated with respect to these minerals already at the beginning of stage 2. Hence, their injection into carbonate rocks with associated pH buffering and increased CO_2(aq) activity easily led to the precipitation of siderite and ankerite. The interaction with the carbonate *Zechstein* rocks appears to be of great importance here. We recall the geological observation that missing *Zechstein* sediments mean the absence of the siderite-ankerite bodies.

Substage 2B. Where the same fluids invaded Permian volcanic or volcanoclastic rocks, they became oxidized and precipitated an assemblage of hematite+Mn oxides and braunite. Oxidation was an effective mechanism for the spatial separation of Fe and Mn observed in the field. According to the known phase equilibria, Fe oxidizes first and hence precipitates first as hematite. The progressive oxidation is further documented by the temporal relationships of the Mn minerals. The precipitation starts with hausmannite ($Mn^{2+/3+}$) and manganite (Mn^{3+}), continues with braunite (silicate of $Mn^{2+/3+}$) and ends with massive precipitation and replacement of pre-existing minerals by pyrolusite (Mn^{4+}).

We must note that rhyolites (or their volcanoclastic equivalents) must have played a special role in the deposition of the oxidized Mn mineralization. They host the Mn minerals in the Thüringer Wald (cf. Fig. 6) but also in the Harz Mts. (Liessmann 2010) or in the Spessart Mts. (Wagner et al. 2010; Fusswinkel et al. 2013, 2014). Hence, this close spatial relationship cannot be overlooked and must be taken into account when one looks for an explanation for the observed mineralizations. The source of manganese for the studied deposits in the Thüringer Wald was sought in the acidic volcanic rocks (Freyberg 1923; Meinel 1993) or in the *Zechstein* Permian sediments (Zimmermann 1924). The Permian volcanic rocks, however, are by no means more enriched in manganese than the siliciclastic sediments and, therefore, their role in the formation of the Mn mineralization must be sought elsewhere. We feel that the ideas presented here do excellently in this respect.

Stage 3. After bleaching of the sandstones, a major illitization event took place (Fig. 13a), dated to middle Jurassic (according to K/Ar dating, Fig. 13b). Illite formed mainly at the expense of feldspars which released a substantial amount of Na, Ca, and Ba into the solution. The released potassium was bound in illite. These fluids formed convection cells within the *Rotliegend* sequence capped by the *Zechstein* sediments (cf. Jowett 1986). In these convection cells, calcite and later barite were precipitating. In the vicinity of the crystalline basement of Thüringer Wald or Thüringer Schiefergebirge, the fluids were also enriched in fluorine and precipitated fluorite. Fluorine was transported in the low-temperature, saline hydrothermal fluid in the form of Ca-F, Na-F or Mg-F complexes (Richardson & Holland 1979) or complexes with organic ligands (Bouabdellah et al. 2013). The presence of organic matter can be assumed with a great certainty because the siliciclastic sediments were in the oil window and are known to be a fertile source of hydrocarbons. There was a limited and local communication with low-salinity waters, documented by a large scatter of fluid inclusion data in some barite samples (especially in *Kamsdorf*). Calcite-barite±fluorite mineralization accompanies both siderite+ankerite and Mn oxide-braunite assemblages and appears to be of regional importance. This type of mineralization is developed similarly

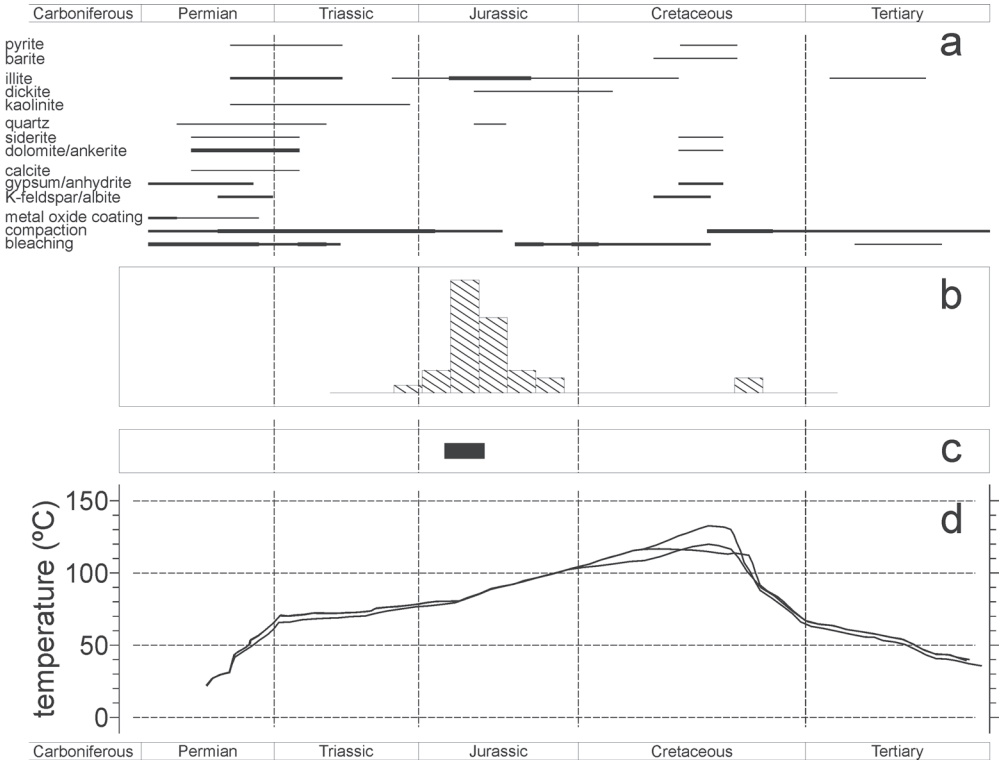

Fig.13. a — Summary and timing of processes (precipitation and dissolution of minerals) which operated in the Permian *Rotliegend* rocks (after Gaupp & Okkerman, their fig.2); **b** — A histogram of K-Ar model ages of illite formation from the German *Rotliegend* rocks (after Gaupp & Okkerman, their fig.9a); **c** — the age of the widespread early to mid-Jurassic hydrothermal event that affected the Rotliegend rocks (Zielinski et al. 2012); **d** — the temperature profile of the Kupferschiefer layer in the Thuringian basin (after Peisker et al. 2013).

in the *Zechstein* sediments and the Permian volcanic/volcanoclastic rocks. This is logical because in this mineralization (i.e., calcite, barite, fluorite), there is little to oxidize or reduce.

Barite is connected without doubt to the extensional period that is manifested in the tectonic record not only in the Thuringian basin but also everywhere in the central European sedimentary basin. The assignment of barite to the extensional phase is based on our structural data (Figs. 3, 4), which show that the barite veins occupy the extensional structures and are cut and offset by the later contractional deformation. According to the observations from the North German Basin, the main period of NE–SW extension lasted from Late Jurassic to Early Cretaceous times (Betz et al. 1987; Ziegler 1987; Kockel 2002) and, therefore, the barite mineralization must be placed in the time interval between the Middle Jurassic and Early Cretaceous.

It is intriguing that the large-scale illitization coincides in time with a major crustal thermal and hydrothermal event, rifting with enhanced heat flow, assumed to occur at ~195–175 Ma (Fig. 13c, Zielinski et al. 2012). This event initiated convective heat transfer within the siliciclastic rocks. The convection cells were capped by the *Zechstein* evaporitic sequences.

Conclusions

Considering the mineralogy of the localities studied, the precipitation sequence, and the temperatures determined by fluid inclusions studied, a link may be found between the fluid evolution in the siliciclastic/volcanic *Rotliegend* sediments (as determined by earlier petrological studies by Gaupp & Okkerman 2011; Peisker et al. 2014; etc.) and the ore mineralizations. There is no doubt that further work must be done to test the ideas presented in this work. The correlation between the two independent data sets, however, provides a striking parallel in terms of the fluid evolution in the siliciclastic sediments and hydrothermal veins in the area studied. Iron and manganese could have been mobilized during the bleaching of the sediments by reduced *Rotliegend* fluids. Iron and manganese were deposited as siderite+ankerite within the *Zechstein* carbonate rocks and as hematite+Mn oxides within the oxidizing environment of the Permian volcanic and volcanoclastic rocks. A Middle-Jurassic illitization event released Ca, Na, Ba, and Pb from the feldspars and Cu, Zn from the mafic minerals into the basinal brines. Calcium and barium precipitated as massive carbonate-barite veins.

Acknowledgements: We thank an anonymous reviewer and J. Zachariáš for their comments and suggestions that significantly clarified, improved and shortened an earlier version of this manuscript. We are grateful to R. Gaupp for fruitful and inspiring discussions about the Rotliegend rocks, B. Kreher-Hartmann (Jena), V. Morgenroth (Schmalkalden) and H. Huckriede (Weimar) for helping us to localize and collect samples. We also wish to thank K. Berger (Kamsdorf),

R. Storch (Trusetal), and F. Veitenhansl (Erfurt) for giving us access to the old mines, unpublished reports, and their knowledge. We thank F. Haubrich (Freiberg) for stable isotope analysis at the laboratory at the TU Bergakademie in Freiberg and his unpublished isotopic data from sulphide minerals from Kamsdorf. Additional thanks go to K. Siewert (Jena) and M. Sattler (Jena) for their help with microthermometry measurement. We are grateful to J. Kley (Jena) for assistance with the structural measurements and his constructive critical comments. This work is a part of INFLUINS, a research project (03IS2091A) funded by the program of "Spitzenforschung und Innovation in den Neuen Ländern" from the German Federal Ministry of Education and Research (BMBF) whose financial assistance is gratefully acknowledged.

References

Andreas D., Kästner H., Seidel G., Wiefel H. & Wunderlich J. 1996: Geologische Karte Thüringer Wald 1:100,000. *Thüringer Landesamt für Geologie*, Weimar.

Baatartsogt B., Schwinn G., Wagner T., Taubald H., Beitter T. & Markl G. 2007: Contrasting paleofluid systems in the continental basement: a fluid inclusion and stable isotope study of hydrothermal vein mineralization, Schwarzwald district, Germany. *Geofluids* 7, 123–147.

Bakker R.J. 2009: Package FLUIDS. Part 3: correlations between equations of state, thermodynamics and fluid inclusions. *Geofluids* 9, 63–74.

Baumann L. & Leeder O. 1969: Paragenetische Zusammenhänge der mitteleuropäischen Fluorit-Baryt-Lagerstätten. *Freiberger Forschung Hefte* C 266, 89–99.

Behr H.J. & Gerler J. 1987: Inclusions of sedimentary brines in post-Variscan mineralizations in the Federal Republic of Germany — a study by neutron activation analysis. *Chem. Geol.* 61, 65–77.

Benkó Z., Molnár F., Lespinasse M., Billström K., Pécskay Z. & Németh T. 2014: Triassic fluid mobilization and epigenetic lead-zinc sulphide mineralization in the Transdanubian Shear Zone (Pannonian Basin, Hungary). *Geol. Carpathica* 65, 177–194.

Betz D., Führer F. & Plein E. 1987: Evolution of the lower Saxony basin. *Tectonophysics* 137, 127–170.

Beyschlag F. 1988: Die Erzlagerstätten in der Umgebung von Kamsdorf in Thüringen. *Jb. Preußisch Geol. Landesanst.* 9, 329–377.

Boness M., Haack U. & Feldmann K.H. 1990: Rb/Sr-Datierung der hydrothermalen Pb-Zn-Vererzung von Bad Grund (Harz), BRD. *Chem. Erde-Geochem.* 50, 1–25.

Boni M., Balassonem G., Fedele L. & Mondillo N. 2009: Post-Variscan hydrothermal activity and ore deposits in southern Sardinia (Italy): selected examples from Gerrei (Silius vein system) and the Iglesiente district. *Period. Mineral.* 78, 19–35.

Bouabdellah M., Castorina F., Bodnar R.J., Banks D., Jébrak M., Prochaska W., Lowry D., Klügel A. & Hoernle K. 2013: Petroleum migration, fluid mixing, and halokinesis as the main ore-forming processes at the Peridiapiric Jbel Tirremi fluorite-barite hydrothermal deposit, northeastern Morocco. *Econ. Geol.* 108, 1223–1256.

Brey-Funke M. 2014: Mineralisierte Fluide im Thüringer Becken. *PhD Dissertation, Friedrich-Schiller University of Jena*, 1–189.

Brosin P. & Veitenhansl F. 2005: Ausgewählte montangeologische, bergtechnische und bergrechtliche Aspekte in der Geschichte des Arlesberger Manganerzbergbaues. *Beiträge Zur Geologie Von Thüringen* 2005, 167–187.

Canals A. & Cardellach E. 1993: Strontium and sulfur isotope geochemistry of low-temperature barite-fluorite veins of the Catalonian Coastel Ranges (NE-Spain) — a fluid mixing model and age constraints. *Chem. Geol.* 104, 269–280.

Charef A. & Sheppard S.M.F. 1988: The Malines Cambrian carbonate-shale-hosted Pb-Zn deposit, France: Thermometric and Isotopic (H, O) evidence for pulsating hydrothermal mineralization. *Miner. Deposita* 23, 86–95.

Clark I.D. & Fritz P. 1997: Environmental Isotopes in Hydrogeology. *CRC Press*, 1–352.

Crespo T.M., Delgado A., Vindel Catena E., López García J.A. & Fabre C. 2002: The latest post-Variscan fluids in the Spanish Central System: evidence from fluid inclusion and stable isotope data. *Mar. Petrol. Geol.* 19, 323–337.

Davis D.W., Lowenstein T.K. & Spencer R.J. 1990: Melting behavior of fluid inclusions in laboratory grow halite crystals in the system NaCl-H_2O, NaCl-KCl-H_2O, NaCl-$MgCl_2$-H_2O and NaCl-$CaCl_2$-H_2O. *Geochim. Cosmochim. Acta* 54, 591–601.

Ding T., Valkiers S., Kipphardt H., DeBievre P., Taylor P.D.P., Gonfiantini R. & Krouse R. 2001: Calibrated sulfur isotope abundance ratios of three IAEA sulfur isotope reference materials and V-CDT with reassessment of the atomic weight of sulfur. *Geochim. Cosmochim. Acta* 65, 2433–2437.

Förster H.J. & Romer R.L. 2010: Carboniferous magmatism. In Linnemann U. & Romer R.L. (Eds.): Pre-Mesozoic Geology of Saxo-Thuringia-From the Cadomian Active Margin to the Variscan Orogen. *Schweizbart*, Stuttgart, 287–308.

Fournier R.O. & Truesdell A.H. 1973: An empirical Na-K-Ca-chemical geothermometer for natural waters. *Geochim. Cosmochim. Acta* 37, 1255–1275.

Franzke H.J. 1992: Bruchprozesse an der Floßberg-Störung bei Ilmenau im Thüringer Wald. *Geol. Bl. NO-Bayern* 42, 69–84.

Franzke H.J. & Schiemenz F. 1980: Die Bruchkinematik des Floßberg-Stechberg-Gangsystems bei Ilmenau im Thüringer Wald. *Z. Angew. Geol.* 26, 547–554.

Franzke H.J., Kapelle G. & Rölling G. 1982: Flächentrendanalyse der Hauptstörungsebene des Floßberg-Stechberg-Mineralgang-systems bei Ilmenau/Thüringer Wald. *Z. Angew. Geol.* 28, 73–76.

Franzke H.J., Ahrendt H., Kurz S. & Wemmer K. 1996: K-Ar Datierungen von Illiten aus Kataklasiten der Floßbergstörung im südöstlichen Thüringer Wald und ihre geologische Interpretation. *Z. Geol. Wiss.* 24, 441–456.

Freyberg B. 1923: Erz- und Minerallagerstätten des Thüringer Waldes. *Verlag von Gebrüder Borntrager*, 97–119.

Fusswinkel T., Wagner T., Wenzel T., Wälle M. & Lorenz J. 2013: Evolution of unconformity-related Mn-Fe-As vein mineralization, Sailauf (Germany): Insight from major and trace elements in oxide and carbonate minerals. *Ore Geol. Rev.* 50, 28–51.

Fusswinkel T., Wagner T., Wenzel T., Wälle M. & Lorenz J. 2014: Red bed and basement sourced fluids recorded in hydrothermal Mn-Fe-As veins, Sailauf (Germany): A LA-ICPMS fluid inclusion study. *Chem. Geol.* 363, 22–39.

Galindo C., Tornos F., Darbyshire D.P.F. & Casquet C. 1994: The age and origin of the barite-fluorite (Pb-Zn) veins of the Sierra del Guadarrama (Spanish Central System, Spain): a radiogenic (Nd, Sr) and stable isotope study. *Chem. Geol.* 112, 351–364.

Gaupp R. & Okkerman J.A. 2011: Diagenesis and reservoir quality of Rotliegend sandstones in the northern Netherlands — a review. In: Grötsch J. & Gaupp R. (Eds.): The Permian Rotliegend of The Netherlands. *SEPM Spec. Publ.* 98, 193–226.

Genter A., Evans K., Cuenot N., Fritsch D. & Sanjuan B. 2010: Contribution of the exploration of deep crystalline fractured reservoir of Soultz to the knowledge of enhanced geothermal systems (EGS). *C. R. Geosci.* 342, 502–516.

Giesemann A., Jäger H.J., Norman A.L., Krouse H.R. & Brand W.A. 1994: On-line sulfur isotope determination using an elemental analyzer coupled to a mass spectrometer. *Anal. Chem.* 66, 2816–2819.

Gleeson S.A., Wilkinson J.J., Shaw H.F. & Herrington R.J. 2000: Post-magmatic hydrothermal circulation and the origin of base metal mineralization, Cornwall, U.K. *J. Geol. Soc. (London)* 157, 580–600.

Hähnel R., Hähnel C., Mädler J., Meinel G. & Wunderlich J. 1995: Strukturelle und stoffliche Entwicklung der anhydritführenden Karbonat-Baryt-Fluorit-Assoziation in der Lagerstätte Hühn (Nordwestlicher Thüringer Wald). *Geol. Jb. Hessen* 123, 5–24.

Halliday A.N. & Mitchell J.G. 1984: K-Ar ages of clay-size concentrates from the mineralisation of the Pedroches Batholitz, Spain, and evidence for Mesozoic hydrothermal activity associated with the breakup of Pangaea. *Earth Planet. Sci. Lett.* 68, 229–239.

Heijlen W., Muchez P.H., Banks D.A., Schneider J., Kucha H. & Keppens E. 2003: Carbonate-hosted Zn-Pb deposits in Upper Silesia, Poland: origin and evolution of mineralizing fluids and constraints on genetic models. *Econ. Geol.* 98, 911–932.

Hurai V., Huraiová M., Slobodník M. & Thomas R. 2015: Geofluids. Developments in Microthermometry, Spectroscopy, Thermodynamics, and Stable Isotopes. *Elsevier*, 1–472.

Hurai V., Harčová E., Huraiová M., Ozdín D., Prochaska W. & Wiegerová V. 2002: Origin of siderite veins in the Western Carpathians I. P-T-X-δ^{13}C-δ^{18}O relations in ore-forming brines of the Rudňany deposits. *Ore Geol. Rev.* 21, 67–101.

Hurai V., Prochaska W., Lexa O., Schulmann K., Thomas R. & Ivan P. 2008: High density nitrogen inclusions in barite from a giant siderite vein: implications for Alpine evolution of the Variscan basement of Western Carpathians, Slovakia. *J. Metamorph. Geology* 26, 487–498.

Johnson C.A., Cardellach E., Tritlla J. & Hanan B.B. 1996: Cierco Pb-Zn-Ag vein deposits: isotopic and fluid inclusion evidence for formation during the Mesozoic extension in the Pyrenees of Spain. *Econ. Geol.* 91, 497–506.

Jowett E.C. 1986: Genesis of Kupferschiefer Cu-Ag deposits by convective flow of Rotliegendes brines during Triassic rifting. *Econ. Geol.* 81, 1823–1837.

Kampschulte A., Buhl D. & Strauss H. 1998: The sulfur and strontium isotopic composition of Permian evaporites from the Zechstein basin, northern Germany. *Geol. Rdsch.* 87, 192–199.

Kießling T. 2007: Die Flussspatgewinnung bei Ilmenau im Thüringer Wald. *Bergbau* 3, 112–120.

Klemm W. 1986: Beiträge zur analytischen Geochemie von Gas-Flüssigkeits-Einschlüssen hydrothermaler Minerale. *Dissertation B, TUBA* Freiberg, 1–72.

Kley J. & Voigt T. 2008: Late Cretaceous intraplate thrusting in central Europe: Effect of Africa-Iberia-Europe convergence, not Alpine collision. *Geology* 36, 839–842.

Kling M. 1995: The ankerite-siderite-sulphide-barite deposit of Kamsdorf (Thuringia, Germany). In: Pašava J., Kříbek B. & Žák K. (Eds.): Mineral Deposits: From their origin to their environmental impacts. *Proceedings of the Third Biennal SGA Meeting, Prague/Czech Republic, Balkema*, Rotterdam, 275–276.

Kockel F. 2002: Rifting processes in NW-Germany and the German North Sea Sector. *Geologie en Mijnbouw* 81, 149–158.

Kornexl B.E., Gehre M., Höfling R. & Werner R.A. 1999: On-line δ^{18}O measurement of organic and inorganic substances. *Rapid Commun. Mass Spectrom.* 13, 1685–1693.

Krahn L. & Baumann A. 1996: Lead isotope systematics of epigenetic lead-zinc mineralization in the western part of the Rheinisches Schiefergebirge, Germany. *Miner. Deposita* 31, 225–237.

Kramm U. & Wedepohl K.H. 1991: The isotopic composition of strontium and sulfur in seawater of late Permian (Zechstein) age. *Chem. Geol.* 90, 253–262.

Kučera J., Muchez P., Slobodník M. & Prochaska W. 2010: Geochemistry of highly saline fluids in siliciclastic sequences: genetic implications for post-Variscan fluid flow in the Moravosilesian Palaozoic of the Czech Republic. *Int. J. Earth Sci.* 99, 269–284.

Kuschka E. & Franzke H.J. 1974: Zur Kenntnis der Hydrothermalite des Harzes. *Z. Geol. Wiss.* 2, 1417–1436.

Lahiry A.K. 1974: Untersuchungen an Flüssigkeitseinschlüssen zur Klärung der paragenetischen Verhältnisse am Beispiel saxonischer Lagerstätten. *Freiberger Forschung Hefte* C 302, 1–95.

Leach D.L., Viets J.G., Kozlowski A. & Kibitlewski S. 1996: Geology, geochemistry and genesis of the Silesia-Cracow zinc-lead district, southern Poland. *Econ. Geol. Spec. Pap.* 4, 70–144.

Liessmann W. 2010: Historischer Bergbau im Harz. *Springer*, 1–470.

Lippmann R., Voigt T., Lützner H., Baunack C. & Föhlisch K. 2005: Geochemische Zyklen im Unteren Muschelkalk (Typusprofil der Jena Formation, Steinbruch Steudnitz). *Z. Geol. Wiss.* 331, 27–50.

Loos G., Saupe M., Mädler U. & Meinel G. 1981: Beitrag zur Klärung der epithermalen Fluoritgenese mit Hilfe der Spurenelementanalyse. *Z. Geol. Wiss.* 27, 567–573.

Lüders V. & Möller P. 1992: Fluid evolution and ore deposition in the Harz Mountains (Germany). *Eur. J. Mineral.* 4, 1053–1068.

McGaig A.M., Tritlla J. & Banks D.A. 2000: Fluid mixing and recycling during Pyrenean thrusting: Evidence from fluid inclusion halogen ratios. *Geochim. Cosmochim. Acta* 19, 3395–3412.

Meinel G. 1993: Die Bildung der Gangmineralisationen Thüringens. *Geowiss. Mitt. Thüringen Beih.* 1, 1–111.

Mertz D.F., Lippolt H.J. & Schnorrer-Köhler G. 1989: Early Cretaceous mineralizing activity in the St. Andreasberg ore district (Southwest Harz, Federal Republic of Germany). *Miner. Deposita* 24, 9–13.

Meyer M., Brockamp O., Clauer N., Renk A. & Zuther M. 2000: Further evidence for a Jurassic mineralizing event in central Europe: K-Ar dating of hydrothermal alteration and fluid inclusion systematics in wall rocks of the Käfersteige fluorite vein deposit in the northern Black Forest, Germany. *Miner. Deposita* 35, 754–761.

Muchez P., Heijlen W., Banks D., Blundell D., Boni M. & Grandia F. 2005: Extensional tectonics and the timing and formation of basin-hosted deposits in Europe. *Ore Geol. Rev.* 27, 241–267.

Munoz M. & Premo W.R. 2005: Sm-Nd dating of fluorite from the worldclass Montroc fluorite deposit, southern Massif Central, France. *Miner. Deposita* 39, 970–975.

Munoz M., Boyce A.J., Courjault-Rade P., Fallick A.E. & Tollon F. 1994: Multi-stage fluid incursion in the Palaeozoic basement-hosted Saint-Salvy ore deposit (NW Montagne Noire, southern France). *Appl. Geochem.* 9, 609–626.

Naden J. 1996: Calcic Brine; a Microsoft Excel 5.0 add-in for calculating salinities from microthermometric data in the system NaCl-$CaCl_2$-H_2O. In: Brown P.E. & Hagemann S.G. (Eds.): *PACROFI VI. University of Wisconsin*, Madison, WI, 87–89.

Nitschke F., Scheiber J., Kramar U. & Neumann T. 2014: Formation of alternating layered Ba-Sr-sulfate and Pb-sulfide scaling in the geothermal plant of Soultz-sous-Forêts. *Neu. Jb. Mineral. Abh.* 191, 2, 145–156.

O'Reily C.O., Jenkin G.R.T., Feely M., Alderton D.H.M. & Fallick A.E. 1997: A fluid inclusion and stable isotope study of 200 Ma of fluid evolution in the Galway Granite, Connemara, Ireland. *Contr. Mineral. Petrology* 129, 120–142.

Peisker J., Voigt T., Aehnelt M. & Köster J. 2013: Rekonstruktion

der Versenkungsgeschichte des zentralen Thüringer Beckens mit Inkolhungswerten aus dem Kupferschiefer. *Beitr. Geol. Thüringen* 20, 121–137.

Piqué A., Canals A., Grandia F. & Banks D.A. 2008: Mesozoic fluorite veins in NE Spain record regional base metal-rich brine circulation through basin and basement during extensional events. *Chem. Geol.* 257, 139–152.

Pratzka G. 1956: Lagerstättengeologische Bearbeitung der Schwerspat- Flußspatlagerstätten in der Umgebung von Trusetal/Thür. *Diploma Thesis*, *Bergakademie Freiberg,* 1–88.

Rauche H. & Franzke H.J. 1990: Stress field evolution at the northern part of the South German Block on the territory of the GDR. *Gerlands Beitr. Geophysik* 99, 441–461.

Richardson C.K. & Holland H.D. 1979: The solubility of fluorite in hydrothermal solutions, an experimental study. *Geochim. Cosmochim. Acta* 43, 1313–1325.

Roedder E. 1984: Fluid inclusions. *Rev. Mineralogy* 12, 1–604.

Rüger F. & Decker H. 1992: Bergbaugeschichte, Geologie und Mineralien des Saalfeld-Kamsdorfer Bergreviers. *Veröff. Museum Gera, Naturw. Reihe* 19, 1–70.

Scheiber J., Nitschke F., Seibt A. & Genter A. 2012: Geochemical and mineralogical monitoring of the geothermal power plant in Soultz-sous-Forêts (France). In: Proceedings of the Thirty-Seventh Workshop on Geothermal Reservoir Engineering. *Stanford University*, SGP-TR-194.

Schmidt-Mumm A. & Wolfgramm M. 2004: Fluid systems and mineralizations in the north German and Polish Basin. *Geofluids* 4, 315–328.

Schröder B. 1987: Inversion tectonics along the western margin of the Bohemian Massif. *Tectonophysics* 137, 93–100.

Schröder N. 1970: Die magmatogenen Mineralisationen des Thüringer Waldes und ihre Stellung im variszischen und saxonischen Mineralisationszyklus Mitteleuropas. *Freiberger Forschung Hefte* C 261, 7–52.

Schwinn G., Wagner T., Baatartsogt B. & Markl G. 2006: Quantification of mixing processes in ore-forming hydrothermal systems by combination of stable isotope and fluid inclusion analyses. *Geochim. Cosmochim. Acta* 70, 965–982.

Slobodnik M., Muchez P.H. & Viaene W. 1994: Variscan and Post-Variscan fluid flow in the Rhenohercynicum of the Ardennes (southern Belgium) and in the eastern part of the Bohemian Massif. *J. Czech Geol. Soc.* 39, 106–107.

Spencer R.J., Möller N. & Weare J.H. 1990: The prediction of mineral solubilities in natural waters: a chemical equilibrium model for the Na-K-Ca-Mg-Cl-SO_4-H_2O systems at the temperatures below 25 °C. *Geochim. Cosmochim. Acta* 54, 575–590.

Spirakis C.S. & Heyl A.V. 1988: Possible effects of thermal degradation of organic matter on carbonate paragenesis and fluorite precipitation in Mississippi Valley-type deposits. *Geology* 16, 1117–1120.

Staude S., Wagner T. & Markl G. 2007: Mineralogy, mineral compositions and fluid evolution at the Wenzel hydrothermal deposit, southern Germany: Implications for the formation of Kongsberg-type silver deposit. *Canad. Mineralogist* 45, 1147–1176.

Staude S., Göb S., Pfaff K., Ströble F., Premo W.R. & Markl G. 2011: Deciphering fluid sources of hydrothermal systems: A combined Sr- and S-isotope study on barite (Schwarzwald, SW Germany). *Chem. Geol.* 286, 1–20.

Steele-MacInnies M., Bodnar R.J. & Naden J. 2011: Numerical model to determine the composition of H_2O-NaCl-$CaCl_2$ fluid inclusions based on microthermometric and microanalytical data. *Geochim. Cosmochim. Acta* 75, 21–40.

Subías I. & Fernández-Nieto C. 1995: Hydrothermal events in the Valle de Tena (Spanish Western Pyrenees) as evidenced by fluid inclusions and trace-element distribution from fluorite deposits. *Chem. Geol.* 124, 267–282.

Symons D.T.A., Kawasaki K., Walther S. & Borg G. 2011: Paleomagnetism of the Cu-Zn-Pb-bearing Kupferschiefer black shale (Upper Permian) at Sangerhausen, Germany. *Miner. Deposita* 46, 137–152.

Thomas R. 1979: Untersuchungen von Einschlüssen zur thermodynamischen und physikochemischen Charkteristik lagerstättenbildender Lösungen und Prozesse im magmatischen und postmagmatischen Bereich. *Dissertation A, TUBA* Freiberg, 1–245.

Toth J.R. 1980: Deposition of submarine crusts rich in manganese and iron. *Bull. Geol. Soc. Am.* 91, 44–54.

Ullrich M.R. & Bodnar R.J. 1987: Systematics of stretching of fluid inclusions II: Barite at 1 atm confining pressure. *Econ. Geol.* 83, 1037–1046.

Verma S.P. & Santoyo E. 1997: New improved equations for Na/K, Na/Li and SiO_2 geothermometers by outlier detection and rejection. *J. Volcanol. Geotherm. Res.* 79, 9–23.

Wagner T. & Lorenz J. 2002: Mineralogy of complex Co-Ni-Bi vein mineralization, Bieber deposit, Spessart, Germany. *Mineral. Mag.* 66, 385–407.

Wagner T., Okrusch M., Weyer S., Lorenz J., Lahaye Y., Taubald H. & Schmitt R.T. 2010: The role of the Kupferschiefer in the formation of hydrothermal base metal mineralization in the Spessart ore district, Germany: insight from detailed sulfur isotope studies. *Miner. Deposita* 45, 217–239.

Werner C.D. 1958: Geochemie und Paragenese der saxonischen Schwerspat-Flußspat-Gänge im Schmalkaldener Revier. *Freiberger Forschung Hefte* C 47, 7–110.

Wickham S.M. & Taylor H.P. 1990: Hydrothermal systems associated with regional metamorphism and crustal anatexis: Example from the Pyrenees, France. In: Geophysics Study Committee: The role of fluids in crustal processes. *National Academy Press*, 96–112.

Wucher K., Steinmüller A. & Puff P. 2001: Geologische Karte von Thüringen 1:25,000; 5334 Saalfeld (Saale). 3rd edition, *TLUG*, Jena.

Zeh A. & Thomson S.N. 2000: Fission-track thermochronology of the Ruhla Crystalline Complex: new contraints on the post-Variscan thermal evolution of the NW Saxo-Bohemian Massif. *Tectonophysics* 324, 17–35.

Zheng Y.-F. 1999: Oxygen isotope fractionation in carbonate and sulfate minerals. *Geochemical J.* 33, 109–126.

Zheng Y.-F. & Hoefs J. 1993: Stable isotope geochemistry of hydrothermal mineralizations in the Harz Mountains. II. Sulfur and oxygen isotopes of sulfides and sulfate and constraints on metallogenetic models. In: Möller P. & Lüders V. (Eds.): Formation of hydrothermal vein deposits. *Monogr. Ser. Min. Deps.* 30, 211–230.

Ziegler P.A. 1987: Late Cretaceous and Cenozoic intra-plate compressional deformations in the Alpine Foreland — a geodynamic model. *Tectonophysics* 137, 389–420.

Zieliński G.W., Poprawa P., Szewczyk J., Grotek I., Kiersnowski H. & Zieliński R.L.B. 2012: Thermal effects of Zechstein salt and the Early to Middle Jurassic hydrothermal event in the central Polish Basin. *AAPG Bulletin* 96, 1981–1996.

Zimmermann E. 1914: Erläuterungen zur Geologischen Karte von Preussen und benachbarten Bundesstaaten 1:25,000; Blatt Saalfeld a. Saale. *Königlich Preußischen Geol. Landesanst.*, Berlin.